Comparison of the CHARM Predictions of the Multirotor Test Bed with Wind Tunnel Experimental Results

Dorsa Shirazi
Aerospace Engineer
NASA Ames Research Center
Moffett Field, CA, 94035

ABSTRACT

Urban air mobility as a fast transportation solution has captured the attention of private companies and government aviation departments in the 21st century. New designs of aerial vehicles are being developed to meet industry needs but often neglect the aerodynamic characteristics and the effects of interacting rotors. This work focuses on predicting rotor behavior and understanding the importance of the rotor wake interaction for future urban air mobility (UAM) designs. The Multirotor Test Bed (MTB) project was initiated at NASA Ames Research center to support the NASA Revolutionary Vertical Lift Technology Project to study rotorcraft performance specifically for multirotor aircraft. The MTB is a modular multirotor test stand that makes testing feasible for up to six rotors at different angles and rotor arrangements, including Tall and Short configurations at different horizontal and vertical rotor separation distances. The MTB was tested in the U.S Army's 7- by 10-Foot Wind Tunnel at NASA Ames Research Center in late 2019. This work focuses on exploring the impact of aerodynamic interactions between the MTB rotors using the Comprehensive Hierarchical Aeromechanics Rotorcraft Model (CHARM) software. The CHARM software is capable of modeling Vertical Take Off and Landing aircraft aerodynamics in maneuvering and steady flight conditions. CHARM allows the user to define flow and body characteristics, including the rotor geometry, aerodynamic conditions, wind tunnel speed, and airfoil tables as inputs. As the first step, a single MTB rotor was simulated in hover, and the results were compared with wind tunnel test data to confirm the CHARM parameters. Once the accurate performance was verified, the MTB rotors were simulated in forward flight, and each rotor was trimmed to the measured thrust. The simulation variables include one, two, four, and six rotors at the Short and Tall configurations, with MTB pitch angles of 0, -5, and -10 degrees. The MTB was simulated with and without wind tunnel walls. These results demonstrate the rotor wake interaction and its impact on rotor performance. This information also helps determine which configurations should be explored for future wind tunnel tests.

NOTATION [1]

c	=	chord length [m]
D	=	drag [N]
L	=	lift [N]
N	=	number of blades
P	=	shaft power [W]
Q	=	torque [N.m]
R	=	rotor radius [ft]
T	=	thrust [N]
θ	=	pitch angle [rad]
μ	=	advance ratio
ρ	=	air density [$\frac{kg}{m^3}$]
σ	=	solidity
Ω	=	rotational speed [rad/s]
C_D	=	drag coefficient
CFD	=	computational fluid dynamics
C_P	=	power coefficient
C_T	=	thrust coefficient
CVC	=	constant vorticity contour
VTOL	=	vertical take-off and landing
FF	=	free field
FM	=	figure of merit
F_x	=	axial force on the load cell [N]
F_z	=	normal force on the load cell [N]
MTB	=	multirotor test bed
M_Z	=	yaw moment
P_i	=	induced power [W]
P_o	=	profile power [W]
RPM	=	revolutions per minute
RVLT	=	Revolutionary Vertical Lift Technology
UAM	=	urban air mobility
UAS	=	unmanned aerial system
WT	=	wind tunnel

Presented at the VFS Aeromechanics for Advanced Vertical Flight Technical Meeting, San Jose, CA, January 25-27, 2022.

INTRODUCTION AND MOTIVATION

For the past two decades, multi-rotor aircraft have been and will continue to be significant contributors to surveillance, search and rescue, resource mapping, and transportation missions, along with a host of further applications. In response to this market need, NASA started to explore experimental multirotor aerodynamic performance in 2015 and 2017 [Ref.1]. Several quadcopters were tested in the U.S. Army 7- by 10-Foot Wind Tunnel at NASA Ames Research Center. The experimental results of the wind tunnel tests have provided scientific information to better understand small Unmanned Aircraft System (sUAS) performance. However, these early experiments had some limitations. For example, the entire aircraft was connected to one load cell, which only allows the measurement of the overall performance of the vehicle. This then provides only limited understanding of the individual aerodynamic behavior of the rotors. In addition, the quadcopter sUAM was manufactured for a fixed rotor distance ratio; therefore, no adjustment was possible to test different rotor distance combinations.

The Multirotor Test Bed (MTB) project was initiated at NASA Ames Research center to support the NASA Revolutionary Vertical Lift Technology (RVLT) Project to study rotorcraft performance specifically for multirotor aircraft. The MTB is a modular multirotor system that makes testing feasible for up to six rotors at different angles and rotor arrangements, including Tall and Short configurations at different horizontal and vertical distances. The MTB project started with the goal of creating a flexible testbed to study multirotor configurations and the performance of each rotor, as well as the aerodynamic interaction and acoustics [Ref.2]. The first test of the MTB system occurred in October 2019 – see Figure 1.

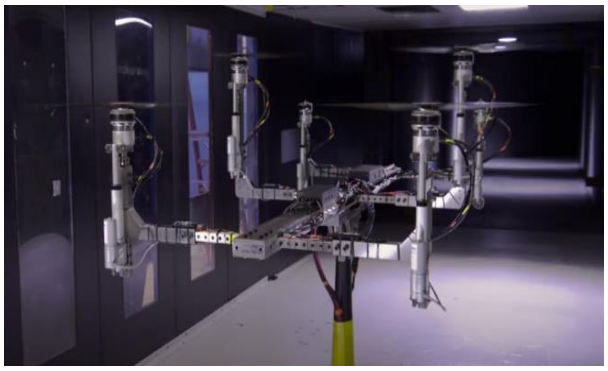

Figure 1. Multirotor Test Bed (MTB) in the 7- by 10-Foot Wind Tunnel at Ames Research Center.

In 2021, the aerodynamic codes CHARM and RotCFD were used to simulate the result of Multirotor Test Bed first wind tunnel entry [Ref.3]. Both analyses simulated the MTB rotors using fixed collective pitch to study any asymmetry in the calculation and validate the capability of both software for quickly predicting the multirotor performance. Since rotors were defined with fixed collective, the computed and measured power could not directly be compared since the computed and measured thrust of each rotor were not matched. This work is focused on trimming the rotors to measured thrust to compare the calculated and measured power directly.

Multirotor Test Bed

The MTB assembly can pitch 20 degrees forward and 10 degrees aft. Each rotor can tilt 90 degrees forward and 5 degrees aft. Further, the MTB assembly allows for adjusting the longitudinal, vertical, and lateral distances. The longitudinal spacing is between 25.5 and 72.0 inches, with the adjustability of 1.5-inch increments. In one-inch increments, the lateral spacing between rotors can change between 24.7 inches to 38.7 inches. The vertical distance can increase 9 inches from the Short configuration to the Tall configuration, with one-inch intermediate increments if desired. The rotor used for the MTB project was a two bladed KDE-CF245-DP with 24.5-inch diameter, Table 1 [Ref.4]. Loads for each rotor are measured using a six-axis load cell. For the wind tunnel test, each load cell was limited to 10-lb of thrust and ± 20 lb of oscillations. Also, each rotor has a rotational speed sensor to record the individual rotor RPM. The rotor numbers, spin directions, and wind direction are shown in Figure 2. Rotors one, four, and five are spinning counter-clockwise. Rotors two, three, and six are turning clockwise to cancel out the torque from rotors one, four, and five.

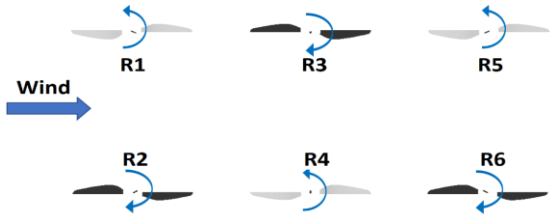

Figure 2. Rotor identification numbers and rotation directions.

Table 1. KDE rotor parameters.

Parameters	Values
Airfoils	KDE-CF245-DP
Radius of blade	1.02 *ft*
Number of blades	2
Average chord	0.13 *ft*
Linear twist rate	-21 *degree/span*
Rotor disk area	3.25 ft^2
Solidity ratio	0.08
Pitch at 75% of the radius	9 *degree*

APPROACH

Test Matrix of the Tunnel Entry

In 2019, the MTB was experimentally evaluated for a matrix of different test rotor case conditions, such as sweeps of rotor RPM, yaw angle, wind tunnel air speed, MTB assembly pitch angle, and number of rotors. The six-rotor case was tested at

the two vertical configurations (Tall and Short) to study the wall effects. For the two-rotor configuration, all rotors were removed except the middle rotors. For the four-rotor case, the back rotors were removed. While many hover cases were tested in 2019 with different numbers of rotors, only one of the hover cases currently was available to use for this study. For the one-rotor case, data was collected at hover using rotor number 2. Table 2 shows the number of rotors and rotor identification numbers that were used for the four different cases. In this study, all the cases were tested at the target rotor speed of 2000 RPM, and wind tunnel speeds of 20 ft/s and 40 ft/s. The lateral and longitudinal distances between the rotors were held constant at 38.7 and 36 inches, respectively. The distance between rotors was measured from the center of each rotor, hub-center to hub-center.

Table 2. 2019 MTB wind tunnel test cases.

Case	Rotor numbers	Configuration
One Rotor	2	Short
Two Rotors	3,4	Short
Four Rotors	1,2,3,4	Short
Six Rotors	1,2,3,4,5,6	Short and Tall

For the purpose of this current research, the test configurations in Table 2 were simulated in CHARM for wind tunnel and free field (no wind tunnel walls) conditions. The MTB support structure was not modeled. The variables considered for the different configurations are presented in Table 3. For the Tall configuration, the rotor hubs were 7 inches higher than the Short configuration with the MTB assembly at 0 deg pitch. The tilt angle of each rotor, independent of the MTB pitch angle, was fixed at 0 deg for all test conditions. Thus, the MTB pitch angle was equivalent to the rotor shaft angle.

Table 3. MTB wind tunnel - test variables.

Variables	Attributes
Pitch Angle [Deg, + aft tilt]	-10, -5, 0
Speed [ft/s]	20, 40
Configuration	Short, Tall
Number of Rotors	1,2,4,6
Rotor speed	2000 RPM
Tip Speed [ft/s]	213.63

Introduction to CHARM

CHARM is a comprehensive Vertical Take Off and Landing (VTOL) aircraft analysis tool developed by Continuum Dynamics Inc (CDI) [Ref.5]. CHARM models the aircraft aerodynamic and dynamic interactions using a combination of Fast Vortex/Fast Panel Solution methods. CHARM uses a grouping scheme in addition to a multipole approximation to decrease the computational time by over two orders of magnitude for 10^5 panels. In the grouping technique, the vertices and panels are grouped into nested cells. For high-density areas, these grids will be more refined. The calculation uses multipole expansion and Taylor series extrapolations. The CHARM software requires less CPU usage and memory compared with high-fidelity computational fluid dynamics (CFD) solvers, therefore, the simulation can be completed in a shorter amount of time and with reduced computational resources. These capabilities make CHARM an appropriate tool for design studies.

CHARM uses Fast Vortex/Fast Panel methods to characterize the rotor aerodynamic behavior, including the rotor/wake interaction and wind tunnel wall effects [Ref.5-7], where the wind tunnel is modeled using inviscid incompressible flow. The 7- by 10- foot wind tunnel test section was defined as a conventional closed tunnel with walls, floor, and ceiling for the MTB simulations in CHARM [Ref.8]. The test section length of the wind tunnel is 15 ft, but in CHARM, the test section length was set to 50 ft (constant section, without contraction or diffuser) to give the simulation enough time to fully develop the flow.

Simulation Conditions in CHARM

The measured parameters in the wind tunnel such as RPM, tunnel speed, and static air density were used in the CHARM simulation. The values for these particular parameters are presented in Appendix A. The airfoil table utilized in the simulation was generated using XFOIL [Refs.3-4]. Also, the rotor locations were defined in three-dimensional space in CHARM, where the X-axis is positive in the opposite direction of airflow (upstream). The Y-axis position is positive for rotors number 1, 3, and 5. Also, the Z-axis is positive downward, see Figure 3. For this study, the MTB test stand was not included in CHARM simulations. The MTB center was about 5/32 inches forward in the positive X-axis direction and 3/16 inches to the right of the tunnel centerline, which was considered when defining the location of each rotor in the CHARM simulation.

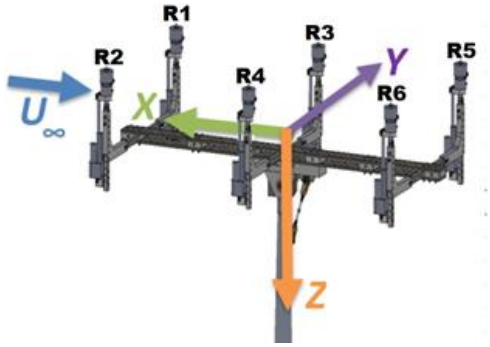

Figure 3. CHARM coordinate system for the MTB.

For all cases, each rotor was trimmed to the measured thrust value. The thrust coefficient (C_T) value for individual rotors was calculated using measured RPM, static density (ρ), and thrust (T) – see Equation. 1. The collective was adjusted to trim the rotor to the measured C_T value within a tolerance of 0.00001. Therefore, the simulation thrust and C_T results will match the measured value well, making it reasonable to compare the power values.

$$C_T = \frac{T}{\rho \pi R^4 \Omega^2} \qquad \text{(Equation 1)}$$

Calculating Aerodynamic Forces and Moments from the 2019 MTB Wind Tunnel Data

The experimental aerodynamic values were calculated using the recorded forces and moments from the six-axis load cells. Each rotor's lift and drag were determined using Equation 2 and Equation 3, where α is the angle between the free stream and the rotor disk, F_x is axial force, and F_z is thrust, with the aerodynamics forces shown in Figure 4. The side force was not counted in the lift and drag calculations. Note that the coordinate system defined in CHARM is different from the load cells' coordinate system.

The torque value was determined directly from the yaw moment, M_z, reading of the loadcells. Also, the power was calculated using the torque and the rotor's angular velocity, Equation 4.

$$L = F_z Cos\alpha - F_x Sin\alpha \qquad \text{(Equation 2)}$$

$$D = F_Z Sin\alpha + F_x Cos\alpha \qquad \text{(Equation 3)}$$

$$P = M_z \, \Omega \qquad \text{(Equation 4)}$$

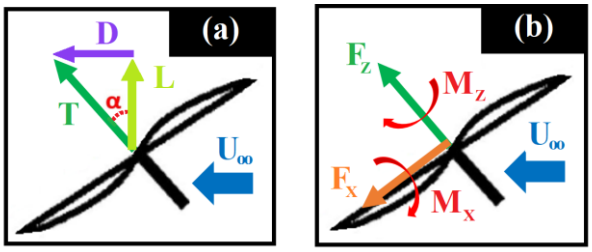

Figure 4. Aerodynamic forces and moments on a rotor disk tilted aft: (a) forces, (b) forces and moments.

KEY RESULTS

First, the isolated rotor simulation result was compared to the experimental data. Then, 24 wind tunnel cases were simulated and compared to preliminary experimental data based on four type variables: MTB pitch angle, forward flight speed (wind tunnel speed), number of rotors, and rotor configuration (vertical distance). There are three pitch angles, two flight speeds, four rotor combinations, and two vertical rotor height configurations (Tall and Short). The study starts with simulation of a single rotor and increases the number of rotors to reach the six-rotor configuration, which is the main focus of this work. The 24 cases were then simulated at the same flight conditions in free field.

Isolated Rotor in Hover

The isolated rotor (Rotor #2) was installed on the MTB and tested in hover in the U.S. Army 7- by 10-Foot Wind Tunnel at Ames Research Center. The only experimental data available for comparison was Run 121, Point 5, with a 0-deg pitch angle at 2001.23 RPM. In CHARM, Rotor #2 was simulated in free field without the presence of any other rotors for a C_T/σ sweep from 0.08 to 0.14.

The figure of merit (FM) and C_P/σ versus C_T/σ plots for the C_T sweep are shown in Figure 5 and Figure 6, respectively, with the single data point also plotted. The CHARM simulation slightly overpredicted the power results compared to the single measured value. Also, the predicted figure of merit values was in the expected range of $0.6 - 0.7$ for the KDE rotor. One hover experimental data point cannot represent the overall performance, particularly the complexity of the unstable wakes generated during hover. Therefore, the experimental data from the single rotor cases at lower wind tunnel speed were used to identify adjustments to the simulation conditions and settings.

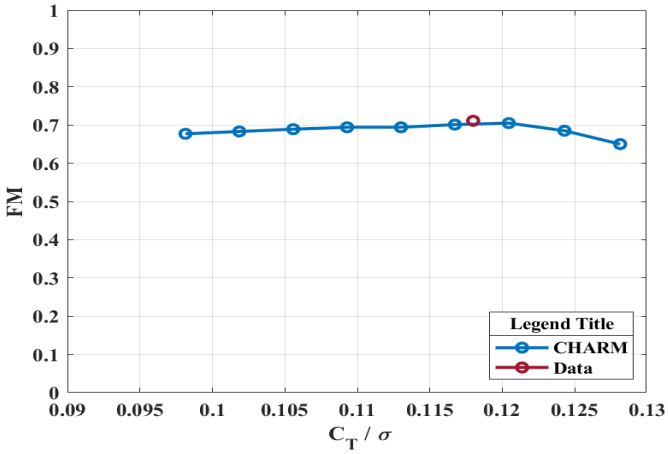

Figure 5. Single rotor in hover – Figure of Merit vs C_T/σ.

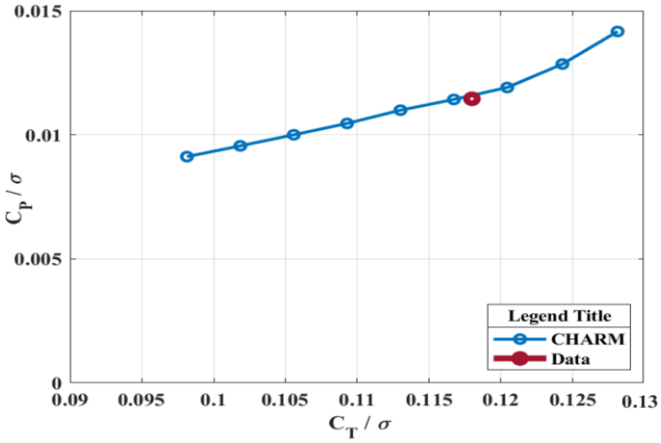

Figure 6. Single rotor in hover – C_P/σ vs C_T/σ.

Single Rotor in Forward Flight

The single KDE rotor (Rotor #2) was trimmed to the measured thrust at 20 ft/s and 40 ft/s for forward flight, and the pitch angles were set to 0, -5, and -10 deg. Figure 7 shows the flow visualization of single KDE rotor in the Short rotor configuration, a -10 degrees pitch angle, and a forward flight speed of 40 ft/s in the wind tunnel. Figure 8 compares experimental data and CHARM wind tunnel predictions for a single rotor for different forward flight speeds. For both speeds, CHARM predicted trends are similar to the measured trends, but magnitudes are overpredicted. However, by

adjusting the coefficient of drag in the airfoil tables, the offset in predicted power values can be reduced.

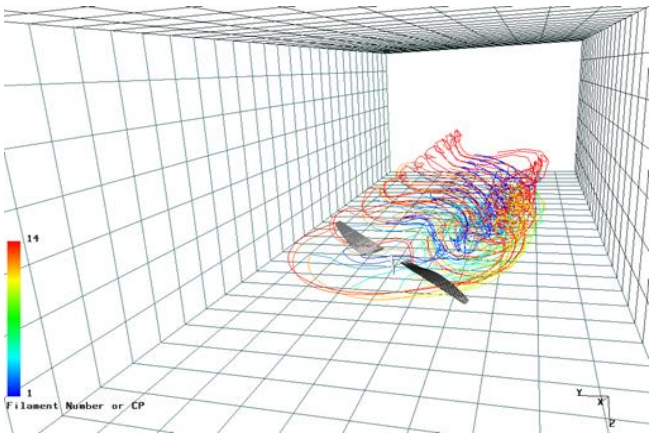

Figure 7. Flow visualization of Rotor #2 in the Short rotor configuration, at -10 deg pitch angle, and a forward flight speed of 40 ft/s in the wind tunnel.

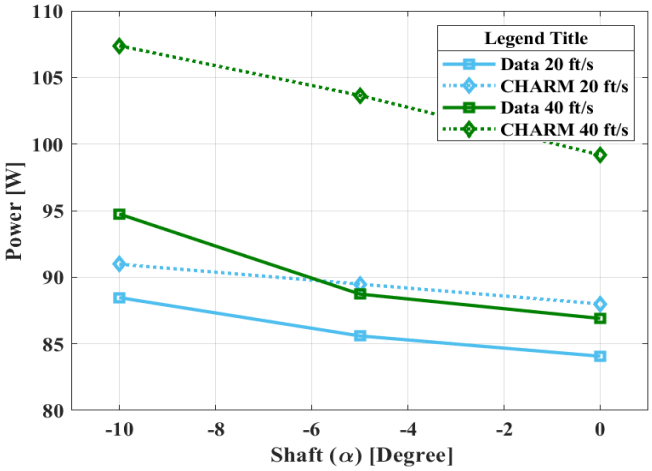

Figure 8. The rotor power values for single rotor cases at wind tunnel in forward flight at 20 and 40 ft/s.

Typically hover experimental data is used to determine adjustments to the airfoil tables, but there were not enough hover data points to use for the MTB. In this case, the experimental data of the lowest forward flight can be used because the advance ratio, μ (see Equation 5), of the measured data at 20 ft/s is less than 0.1, which indicates the aerodynamic value such as profile power will be similar to a hover data.

$$\mu = \frac{V}{R\Omega} \qquad \text{(Equation 5)}$$

Airfoil Table Corrections

The airfoil drag can influence the shaft power prediction, so establishing the correct minimum drag coefficient for the airfoil is important. To find the relation between the power and C_d, the expression in Equation 6 is used,

$$dP = \Omega dQ \qquad \text{(Equation 6)}$$

$$dP = \Omega N F_X r dr$$

where dP is the section power and dQ is the sectional torque. The sectional torque is associated with the linear inplane force, F_X, the torque arm of length, rdr, and the number rotor blades, N. With the assumption of a small inflow angle, the inplane force can be defined as, $L\,\theta + D$, which makes the sectional power equal the summation of the induced power (P_i) and the profile power (P_o), as presented in Equation 7.

$$dP = \Omega N (L\,\theta + D)\, rdr$$

$$dP = \Omega N L\,\theta + \Omega N D r dr$$

$$dP = P_i + P_o \qquad \text{(Equation 7)}$$

The sectional profile power is defined by

$$dP_o = \Omega N D r dr \qquad \text{(Equation 8)}$$

where D is the sectional drag given by the expression in Equation 9.

$$D_{section} = \frac{1}{2}\rho(\Omega r)^2 c\, c_d \qquad \text{(Equation 9)}$$

The sectional profile power is defined,

$$dP_o = \Omega N \frac{1}{2}\rho(\Omega r)^2 c\, c_d\ rdr$$

The profile power can then be calculated using Equation 10, with the assumptions that chord length is constant, blade twist is linear, and the c_d is constant.

$$P_o = \int_{r=0}^{r=1} \frac{1}{2}\rho\, c_d\, \Omega^3\, r^3 N c\, dr$$

$$P_o = \frac{1}{2}\,\frac{R^4}{4}\,\Omega^3 N c\, \rho\, c_d$$

$$P_o = \frac{1}{8} c_d \rho c N \Omega^3 R^4 \qquad \text{(Equation 10)}$$

The power coefficient (C_P) can be determined by:

$$C_P = \frac{P}{\rho A(\Omega R)^3}$$

So, the coefficient of the profile power can be calculated using Equation 11, where A is the rotor disk area and the P_o is defined as Equation 10.

$$C_{P_o} = \frac{P_o}{\rho A(\Omega R)^3} \qquad \text{(Equation 11)}$$

$$C_{P_o} = \frac{\frac{1}{8} c_d \rho c N \Omega^3 R^4}{\rho A(\Omega R)^3}$$

$$C_{P_o} = \frac{c_d c N R}{8R^2\pi}$$

Note that the ratio between the rotor blade area and rotor disk area, $\frac{cNR}{R^2\pi}$, is solidity σ.

$$C_{P_o} = \frac{\sigma\, c_d}{8} \qquad \text{(Equation 12)}$$

The amount of adjustment for the c_d value can be calculated using the delta total power (ΔP) between the measurement and prediction values with assumption of having constant c_d value as presented in Table 4. The average of the c_d at forward flight of 20 ft/s is ~ 0.0039, which suggests adjusting the $c_d$values of the airfoil tables by increment of -0.003 or -0.004 increment.

Table 4. Using the total power to determine the required C_d increment to correct the airfoil table.

V [ft/s]	Pitch [Deg]	Data Power	CHARM Power	ΔP	c_d
20.30	-10	88.47	90.98	2.51	0.0028
20.40	-5	85.59	89.48	3.90	0.0044
20.37	0	84.06	87.99	3.9284	0.0044

Also, the $P_i + P_o$value can be used in Equation 10 instead of the total power to calculate the c_d increments. For CHARM, the P_i and P_o is obtained directly from the simulation results, but, the profile power and the induced power for the data cannot be determined directly from the load cells force and moment, so the $P_i + P_o$ can be determine using the Equation 13, where P is the total power, D is drag and V is the forward flight speed.

$$P_i + P_o = P + DV \qquad \text{(Equation 13)}$$

Using the $\Delta(P_i + P_o)$, the c_d values were calculated for forward flight of 20 ft/s, Table 5, and the average c_d was ~0.0051, which suggests adjusting the $c_d$values of the airfoil tables by +0.005.

Table 5. Using the $P_i + P_o$ to determine the required c_d increment to correct the airfoil table.

V [ft/s]	Pitch [Deg]	Data $P_i + P_o$	CHARM $P_i + P_o$	$\Delta(P_i + P_o)$	c_d
20.30	-10	82.72	82.03	0.69	0.0008
20.40	-5	89.78	82.03	7.76	0.0087
20.37	0	94.51	89.48	5.03	0.0057

To determine which c_d increment is reasonable to use for the airfoil table adjustment, the Δc_d of -0.003, -0.004, -0.005, and +0.005 were applied to the airfoil tables to simulate the single rotor at forward flight of 20 ft/s and pitch angles of -10, -5 and 0 degrees. Figure 9 shows the comparison of the power versus the pitch angle for data and the trimmed rotor with: Δc_d=0 (no c_d changes), Δc_d= -0.003, Δc_d= -0.004, Δc_d= -0.005 and Δc_d= +0.005. The power comparison shows that the Δc_d= -0.003 improves the prediction of the power at forward flight of 20 ft/s. In addition, observing the simulation results for $P_i + P_o$ versus pitch angle could provide more information to help identify the preferable increment for the airfoil, see Figure 10.

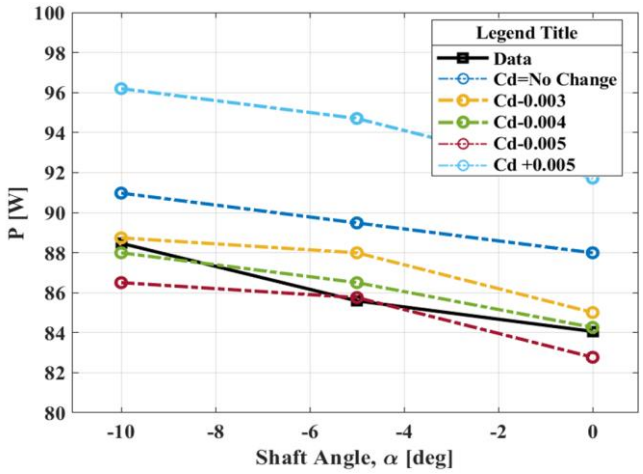

Figure 9. The comparison of the data power versus the CHARM with different Δc_d - single rotor cases in the wind tunnel at 20 ft/s.

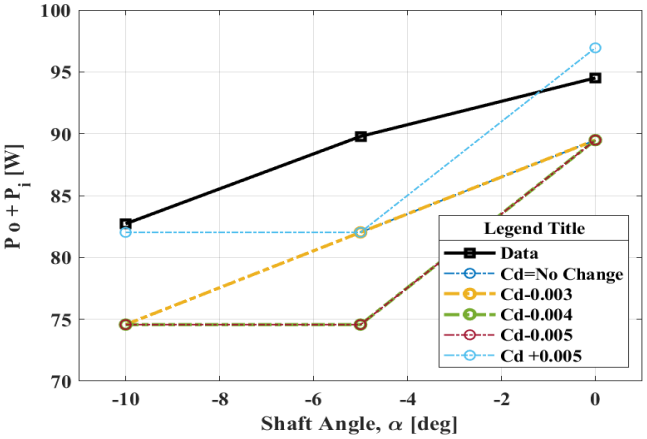

Figure 10. The comparison of the data $P_i + P_o$ versus the CHARM with different Δc_d - single rotor cases in the wind tunnel in forward flight at 20 ft/s.

In Figure 10, the trend using Δc_d= -0.003 is similar to the data, though still offset, is selected as the more appropriate increment for adjusting the drag coefficient for the lower forward flight speed. Also, observing the simulation results for drag versus pitch angle shows that calculated rotor drag is not sensitive to airfoil drag increment, see Figure 11. According to these results, the induced power may be over-predicted at forward flight. Overall, there is insufficient information to identify the exact drag value, and the conclusion was drawn from the available information. The purpose of this exercise was to gain some insight into the possible sources of the differences between measured and calculated rotor power in forward flight. The airfoil tables, developed by CFD analysis for the sections and Reynolds number of the KDE blades, have very high drag coefficient values, so an over-estimate of the drag by Δc_d= -0.003 would not be unreasonable. For the rest of this paper, except where noted, all CHARM results are being trimmed to the measured thrust, and the $c_d$values in the airfoil table were corrected with an increment of -0.003. For the limited fixed collective results

presented, the rotor was not trimmed, and the drag in the airfoil table was not corrected (that is, $\Delta c_d = 0$).

By trimming the rotor to the measured thrust, CHARM kept adjusting the collective angle until the measured C_T value was reached. The CHARM collective angle prediction is shown in Figure 12 for the single rotor at the pitch angle of -10, -5, and 0 deg at wind tunnel speeds of 20 ft/s and 40 ft/s. All rotors in the MTB experiment were operated at fixed, 0-deg collective. Figure 12 shows a -1-deg shift in collective values. This offset could be caused by different definitions of the blade pitch axis between experiment and simulation that can affect the collective pitch setting. Differences in actual and measured blade twist or the zero-lift angle of the airfoil table can also contribute to the offset.

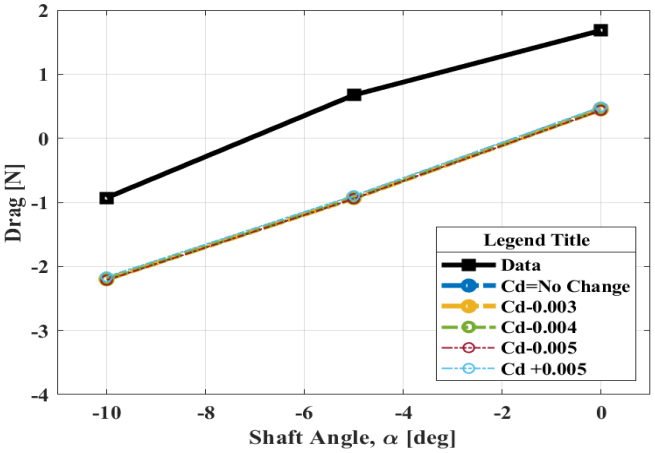

Figure 11. Effect of different Δc_d on CHARM drag predictions. Single rotor (Rotor #2) cases in the wind tunnel for forward speed of 20 ft/s.

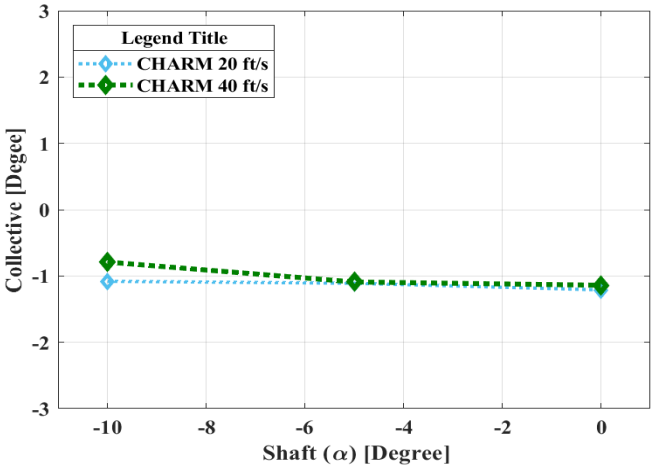

Figure 12. Predicted rotor collective values after applying Δc_d= -0.003 to the airfoil tables. Single rotor (Rotor #2) cases in the wind tunnel for forward speeds of 20 ft/s and 40 ft/s.

Figure 13 and 14 shows thrust and power results for the single rotor at forward speed of 20 and 40 ft/s inside the wind tunnel, after adjusting the c_d values in the airfoil tables by an increment of -0.003. As was expected, the power prediction for 20 ft/s was improved more than predictions for 40ft/s. The power prediction at the higher speed was still improved compared to using uncorrected airfoil tables.

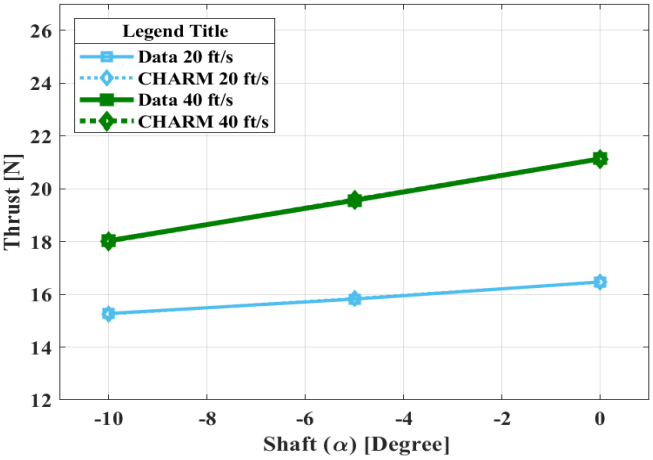

Figure 13. Predicted rotor thrust values after applying Δc_d= -0.003 to the airfoil tables. Single rotor cases in the wind tunnel for forward speeds of 20 and 40 ft/s.

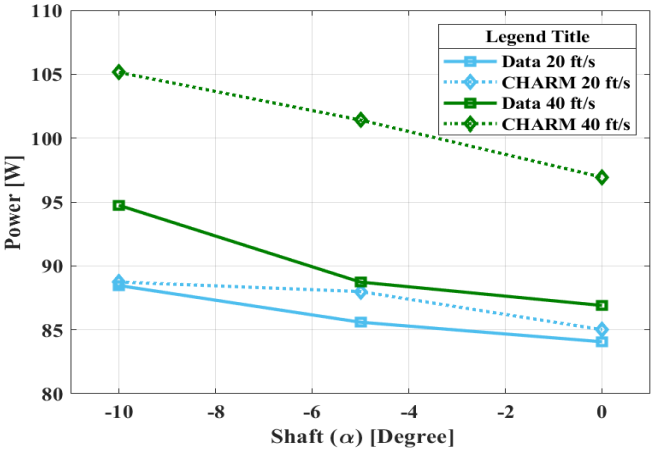

Figure 14. Predicted rotor power values after applying Δc_d= -0.003 to the airfoil tables. Single rotor cases in the wind tunnel for forward speeds of 20 and 40 ft/s.

Table 6. Discrepancy between predicted and measured power for one MTB rotor (Rotor #2).

V [ft/sec]	Pitch [Deg]	Power Dis% of Rotor #2
20.30	-10	-0.31
20.40	-5	-2.80
20.37	0	-1.12
39.83	-10	-10.98
39.33	-5	-14.29
39.34	0	-11.55

For the one-rotor case (Rotor #2), the discrepancy between the experimental data and CHARM was calculated at the pitch angle of -10, -5, and 0 degrees for wind tunnel speeds of 20 ft/s and 40ft/s, see Table 6. These results show that with the drag coefficient adjustment, CHARM overpredicts the power for the single rotor at wind tunnel speed of 20 ft/s by less than 3%, with a larger overprediction at 40 ft/s.

Two Rotors in Forward Flight

Two rotors were trimmed and simulated in the wind tunnel in forward flight for 20 ft/s at pitch angles of 0, -5, and -10 degrees. The two rotors selected for these runs Rotor #3 and #4, located at the middle of the MTB structure test stand. The collective prediction for the two-rotor case is shown in Figure 15 at the pitch angle of -10, -5, and 0 deg at a wind tunnel speed of 20 ft/s. Any variation of the collective prediction from -1 deg (see Figure 12) reflects the influence of wake interference and unsteadiness on the thrust prediction.

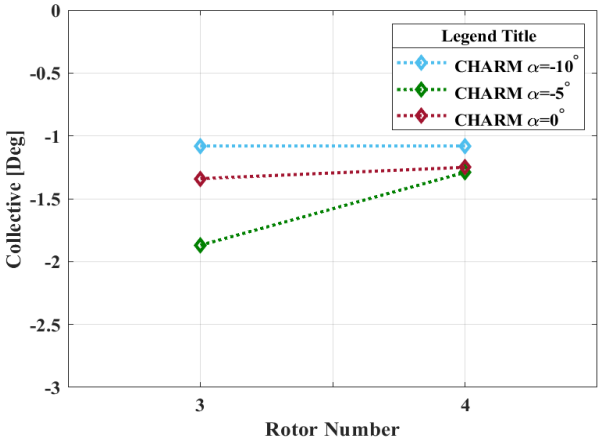

Figure 15. The collective values for individual rotors at pitch angle of -10, -5, and 0 deg, for two-rotors in the wind tunnel in forward flight of 20 ft/s.

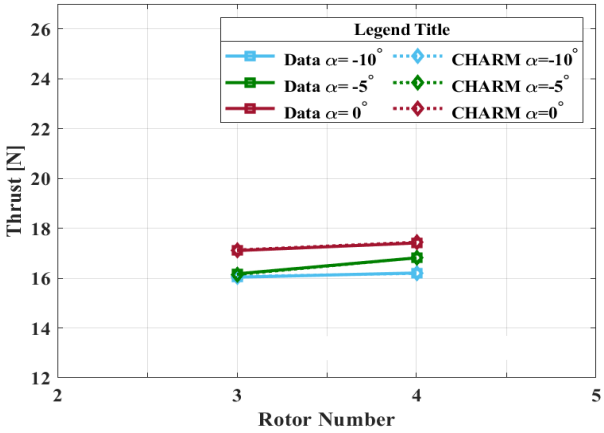

Figure 16. Measured and computed thrust values for individual at pitch angle of -10, -5, and 0 deg, for two-rotor case in the wind tunnel at speed of 20 ft/s.

These collective results show asymmetry between Rotor #3 and Rotor #4 for the pitch angle of -5 degrees, similar to the measured thrust trend shown in Figure. 16; the CHARM prediction follows this trend. Since Rotor #4 has the highest collective prediction and measured thrust at a -5 deg pitch angle, it was also expected to have the highest power measured at this pitch angle compared to Rotor #3. These trends could be due to the effects of interference in measurement data. The simulation results for average thrust and power are compared to the wind tunnel experimental data in Figure 16 and Figure 17. Flow visualizations are included in Appendix B. For the two-rotor case, the thrust and power values are expected to be very similar for Rotor #3 and Rotor #4 due to the absence of the front rotor and less rotor wake interaction. However, the measured power and CHARM prediction shows a difference of magnitude between Rotor #3 and Rotor #4 with a negative correlation. The difference between the predicted and measured average power is largest for the 0 deg case. That the trend of the power difference between the two rotors is reversed between prediction and measurement perhaps reflects randomness in the aerodynamic source of this asymmetry.

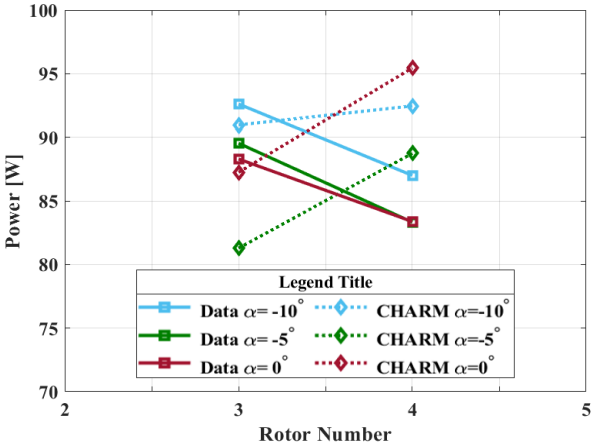

Figure 17. Measured and computed power values for individual at pitch angle of -10, -5, and 0 deg, for two-rotor case in the wind tunnel at speed of 20 ft/s.

Table 7. Discrepancy between measured power and CHARM prediction power - based on last rotor revolution for two-rotor case.

V [ft/s]	Pitch [º]	Power Discrepancy% Rotor #3	Rotor #4
20.30	-10	1.77	-6.28
20.42	-5	9.22	-6.50
20.44	0	1.19	-14.48

The discrepancy between the experimental data and CHARM for the individual rotors was calculated at the pitch angle of -10, -5, and 0 degrees and presented in Table 7. These results show that CHARM over-predicts the power for Rotor #4 and underpredict for Rotor #3. Overall, trimming the rotor to the measured thrust and adjusting the c_d values in the airfoil tables improved the power prediction compared to running the simulation at fixed collective and without adjusting the c_d values in the airfoil tables. The discrepancy between the experimental data and CHARM for the individual rotor was calculated, then the average discrepancy at each pitch angle was recorded, Table 8. These results show that the two-rotor case at the pitch angle of -10, -5, and 0 degrees have the discrepancy of 4.03%, 7.86%, and 7.83%, respectively. The summation of the experimental and CHARM predictions power at different pitch angles are presented in Appendix C.

Table 8. The average discrepancy of power between the CHARM prediction and experimental data for two MTB rotors at the wind tunnel in forward flight testing at speed of 20ft/s.

c	Pitch [°]	Power Ave. Discrepancy%
20.10	-10	4.03
19.96	-5	7.86
19.62	0	7.83

These simulation cases are run for 50 revolutions, but Figure 16 and Figure 17 show the result of the last revolution. Figure 18 shows the power value of two-rotor cases at -10, -5, 0 deg pitch angle at the last ten revolutions. Using the average power over the previous last ten revolutions can improve the power prediction of Rotor #4 at 0 deg pitch angle from discrepancy -14.48% to -6.44%, see Table 9.

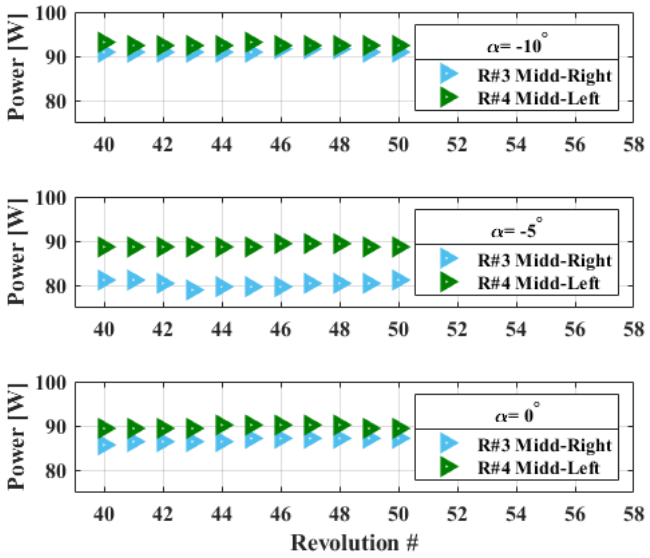

Figure 18. CHARM power variation over last 10 rotor revolutions: pitch angle of -10, -5, and 0 deg; 20 ft/s; Rotors 3 and 4.

Table 9. Discrepancy between measured power and CHARM average power - based on last ten rotor revolutions - for two-rotor case.

V [ft/sec]	Pitch [Deg]	Power Discrepancy% Rotor #3	Rotor #4
20.30	-10	1.77	-6.28
20.42	-5	10.46	-6.50
20.44	0	1.19	-6.44

Four Rotors in Forward Flight

The Four-rotor configuration was tested at 20 ft/s forward flight speed. Rotor #1, #2, #3 and #4 were installed on the MTB and data were collected at pitch angles of 0, -5, and -10 degrees. For the CHARM simulations, the airfoil tables were adjusted by Δc_d= -0.003, and each rotor was trimmed to the individual measured rotor thrust. Simulation results for collective, thrust and total power are compared with experimental data at 0, -5, and -10 degrees pitch angles for each rotor, shown in Figure 19, Figure 20 and Figure 21, respectively.

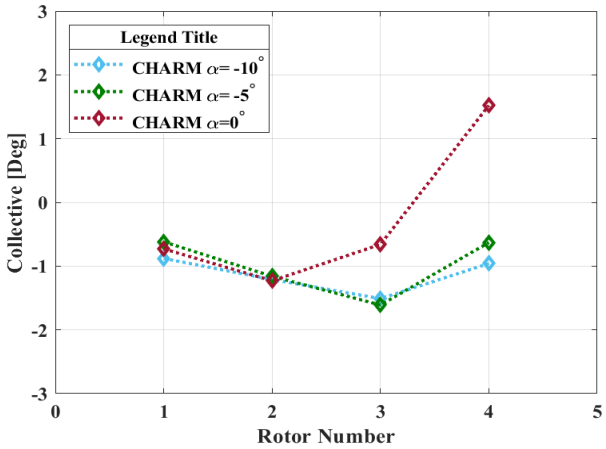

Figure 19. The collective values for individual rotors at 20ft/s and pitch angle of -10, -5, and 0 deg, for four-rotors.

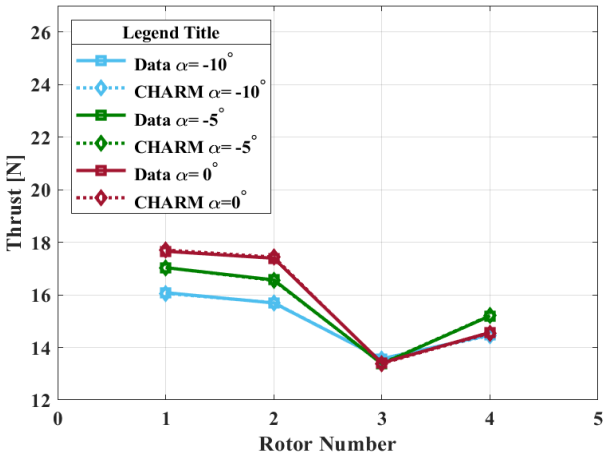

Figure 20. Measured and computed thrust values for individual rotors at 20 ft/s and pitch angle of -10, -5, and 0 deg for four-rotors.

The measured values show that the back rotors generate less thrust than the front rotors (see Figure. 20) while requiring more power (see Figure. 21), which was expected due to rotor wake interference. Rear rotors experienced lower thrust due to the downwash from the front rotors. The power change was due to the change of induced velocity from the front rotors and the change in thrust value. The power prediction at the -5 and -10 deg pitch angle are following the thrust data suggesting power is more influenced by the thrust; even so, the collective and power values are out of trend for the 0 deg pitch angle. The discrepancy between the CHARM prediction and experimental data for each rotor is tabulated for 20 ft/s at the pitch angle of -10, -5, and 0 degrees, see Table 10. The power prediction for Rotor #4 at 0 deg pitch angle is out of trend which requires further study. The average discrepancy at each pitch angle and the summation

of power for the experimental and CHARM predictions at different pitch angles is presented in Appendix C.

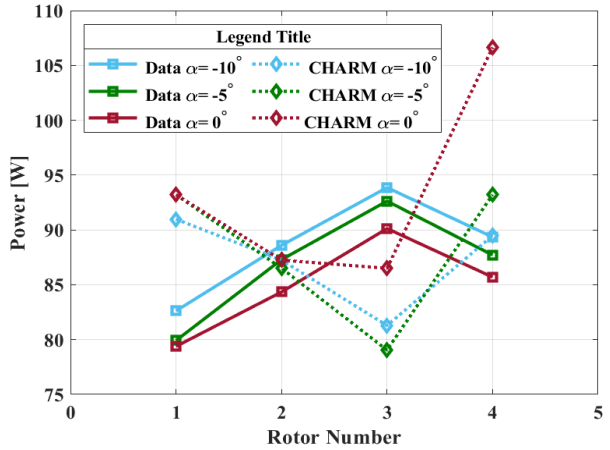

Figure 21. Measured and computed power values for individual rotors at 20 ft/s and pitch angle of -10, -5, and 0 deg for four-rotors.

Figure 22 shows the power prediction versus measured value for the four-rotor case where the rotor rotation direction has been changed compared to Figure 21. The rotor rotation direction was set to clockwise for Rotor #1 and #4 and counter-clockwise for Rotor #2 and #3. It was expected to see minor thrust and power value changes since changing the rotor direction should not influence the average power and thrust prediction. Nevertheless, these results show that CHARM prediction for Rotor #4 improved ~ 13% at 0 deg pitch angle, while the power prediction at the pitch angle of -5 deg has a ~10% higher discrepancy. This result indicated the presence of unsteady wake in the simulation.

Table 10. Discrepancy between measured power and CHARM average power for four-rotor case.

		Power Discrepancy%			
V [ft/s]	Pitch [º]	R #1	R #2	R #3	R #4
20.30	-10	-10.11	1.52	13.40	-0.15
20.42	-5	-16.64	0.91	14.66	-6.27
20.44	0	-17.43	-3.45	4.02	-24.43

In order to investigate this unsteady behavior, the power prediction of the individual rotor for the four-rotor case at 0 deg pitch angle was plotted for the last ten revolutions, see Figure 23. These results validate the presence of the unsteady wake in the simulation. Additional figures for power versus revolution number for four-rotor cases at -10 and -5 deg pitch angles are included in Appendix D. All the simulation cases in this study were run for 50 revolutions; however, the result of the last revolution was used for Figures 19-22. Averaging the power over the last ten revolutions can improve the results for Rotor #4 at 0 deg pitch angle from discrepancy -24.43% to -17.38% The unsteady wake may occur due to the presence of the wind tunnel walls in the simulation. Figure 24 presents the power values for the last ten revolutions at 0 deg pitch angle with no wind tunnel walls and forward speed of 20 ft/s.

The difference between Figure 23 and Figure 24 reveals the effect of the walls on the simulation results, especially for Rotors 3 and 4.

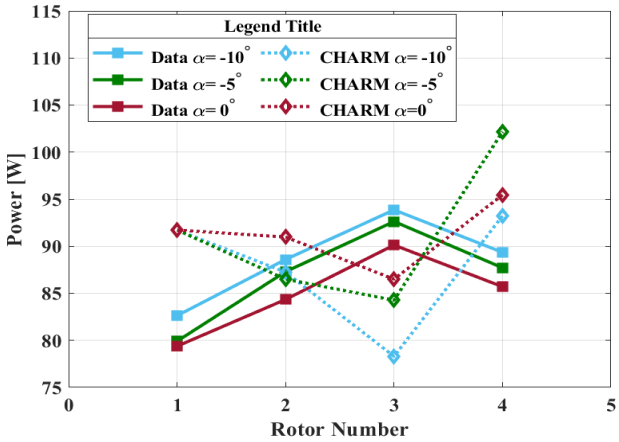

Figure 22. Measured and computed power values for four-rotor case after changing the rotor rotation direction in CHARM at 20 ft/s and pitch angle of -10, -5, and 0 deg.

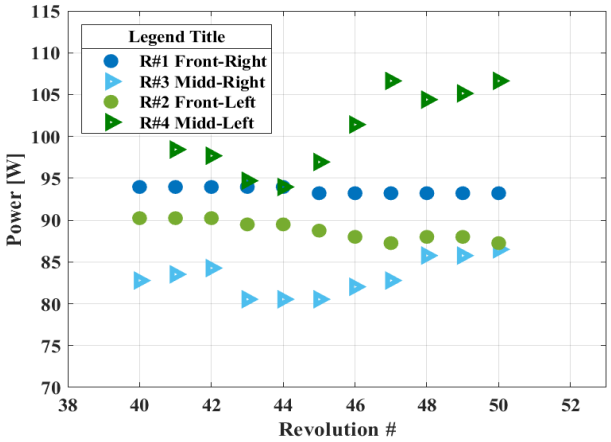

Figure 23. CHARM power variation over last 10 rotor revolutions (total 50 revolutions) with wind tunnel walls: pitch angle of 0 deg; 20 ft/s; Rotors 1, 2, 3 and 4.

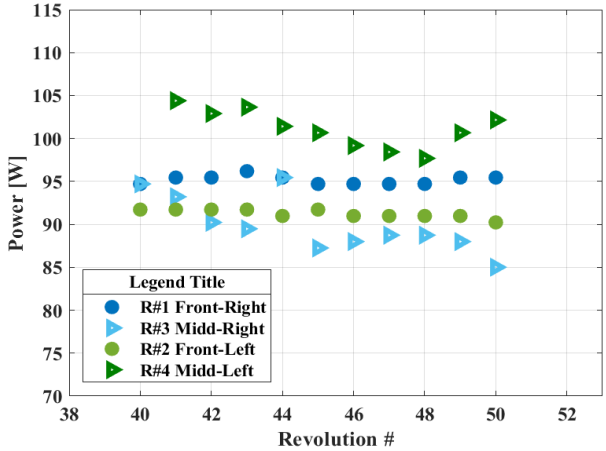

Figure 24. CHARM power variation over last 10 rotor revolutions (total 50 revolutions) without wind tunnel walls: pitch angle of 0 deg; 20 ft/s; Rotors 1, 2, 3 and 4.

Also, Figure 25 and Figure 26 show the wakes of the four rotors at a pitch angle of 0 and -10 degrees in the Short configuration in the test section. Wakes from the front rotors interact with the back rotors, but, as was expected at -10 deg pitch angle, these wake interactions decreased. Additional figures for four-rotor cases at different pitch angles are included in Appendix B.

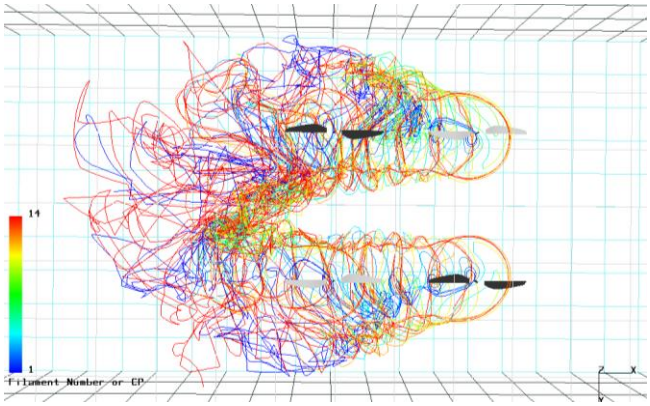

Figure 25. Four-rotor cases at forward flight 20 ft/s in wind tunnel with pitch 0 degrees.

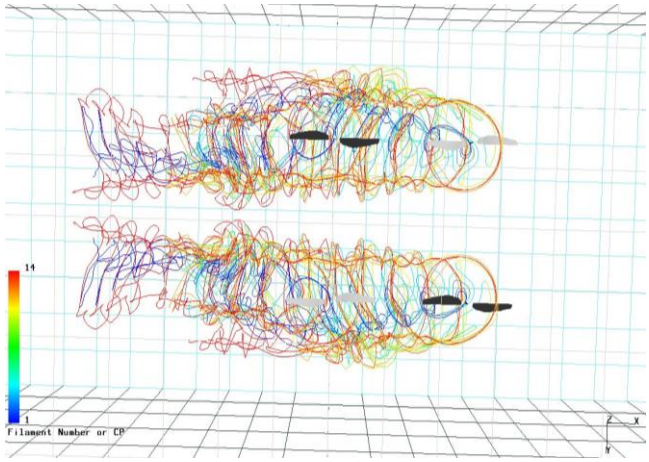

Figure 26. Four-rotor cases at forward flight 20 ft/s in wind tunnel with pitch -10 degrees.

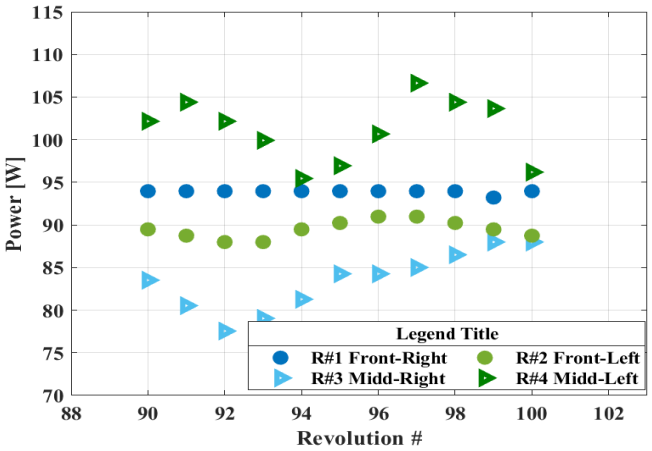

Figure 27. CHARM power variation over last 10 rotor revolutions (total 100 revolutions) with wind tunnel walls: pitch angle of 0 deg; 20 ft/s; for four-rotor case.

Increasing the number of rotor revolutions for the simulation can influence the power prediction result. Figure 27 shows the last ten power values out of 100 revolutions for the four-rotor case at 0 deg pitch angle. These results still have evidence of the unsteady wake. Figure 28 provides a comparison of cases that were run for the four- rotor case at 0-deg pitch angle. The power result presented belongs to the last revolution of each run. These results indicate that increasing the number of revolutions in the simulation can improve the result of power prediction for Rotor #4 at 0-deg pitch angle. but not for the other rotors or other pitch angles. These results indicate that the wake interactions of a multirotor configuration are quite complex. Further study is required to examine the data and explore CHARM simulation options in more detail to understand the rotor wake interference better.

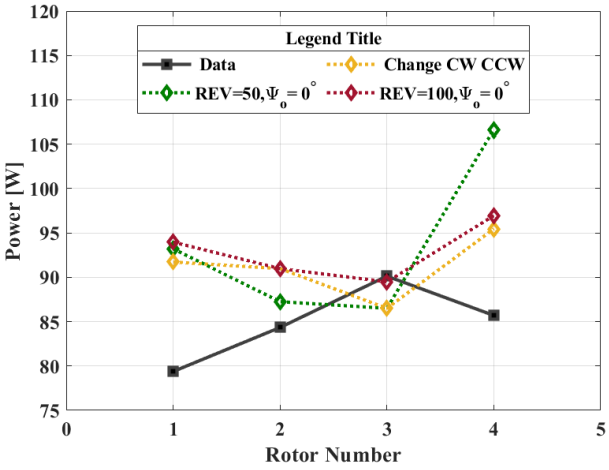

Figure 28. The power prediction for Rotor #4: pitch angle of 0 deg; 20 ft/s; for four-rotor case.

Six Rotors in Forward Flight

Simulations of the six-rotor configuration were performed for both the Short and Tall configurations. At a 0-deg pitch angle, the rotor distance from the ceiling for the Tall and Short configuration were 1.66 ft and 2.45 ft, respectively. Changing the pitch angle brings Rotor #5 and Rotor #6 closer to the ceiling, while Rotor #1 and Rotor #2 move further from the ceiling and closer to the floor. These simulation cases are run for 50 revolutions, but Figures 29-41 show the result of the last revolution.

Results for the Six-Rotor, Short Configuration

The measured thrust and power, along with CHARM predicted for the six-rotors in the Short configuration at the pitch angles of 0, -5, -10 deg at 20 and 40 ft/s are shown, respectively, in Figures 30-33. Also, the corresponding collective values in forward flight speed of 20 and 40 ft/s were shown in Figure 29. Figure 30 and Figure 31 show that the measured thrust between left and right rotors is not that different for the front rotors (Rotors 1 and 2), but still, the measured power and predicted show an asymmetric effect at forward speed of 20 ft/s. These results indicate that CHARM underpredicts the power at forward flight speed of 20 ft/s and

overpredicts at 40 ft/s, as shown in Table 11. The results presented in Figure 31 show that the highest power reading was achieved at a pitch angle of -10 deg in both the experimental data and CHARM; the result was contrary to expectations that at -10 deg, the wakes of the front rotors were expected to interact less with the downstream rotors, as shown in Figure 34. Rotor wake interactions had less impact on aerodynamic performance at -5 and -10 deg pitch angles. Comparatively, the wakes of the front rotors at pitch angle of 0 deg caused a wake roll-up with the wakes of the middle and back rotors. Additional wake figures for six-rotor cases is included in Appendix B.

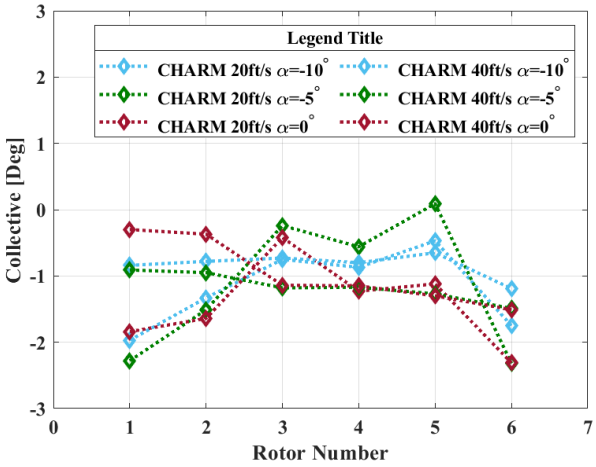

Figure 29. The collective values for individual rotors at pitch angle of -10, -5, and 0 deg, for six-rotors, Short configuration in forward flight of 20 ft/s and 40 ft/s.

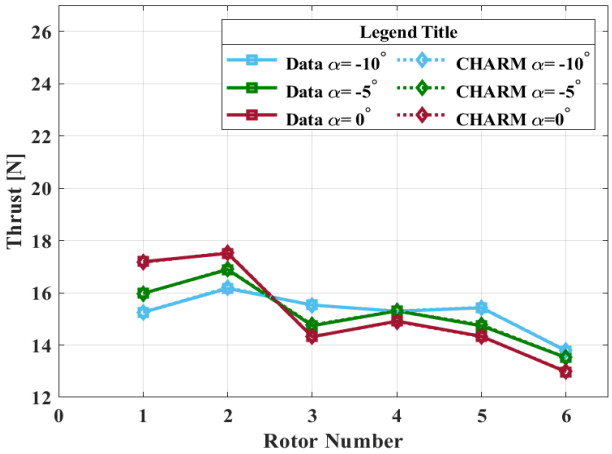

Figure 30. Measured and computed thrust values for individual rotors at 20 ft/s and pitch angle of -10, -5, and 0 deg for six-rotors, Short configuration.

The discrepancies between the experimental data and CHARM for the individual rotors at -10, -5, and 0 deg pitch angles are presented in Table 12. These calculated discrepancies show a lower average discrepancy at the lower tunnel speed of 20 ft/s. This behavior was much more pronounced at the pitch angle of 0 degrees where the average discrepancy changed from 5.96% to 11.93% when forward speed increased from 20 ft/s to 40 ft/s.

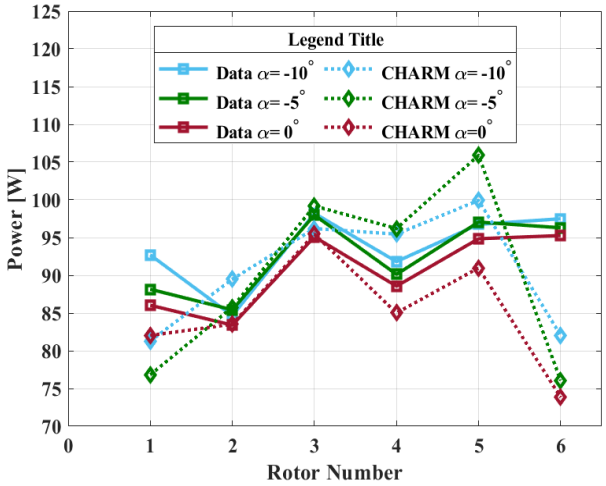

Figure 31. Measured and computed power values for individual rotors at 20 ft/s and pitch angle of -10, -5, and 0 deg for six-rotors, Short configuration.

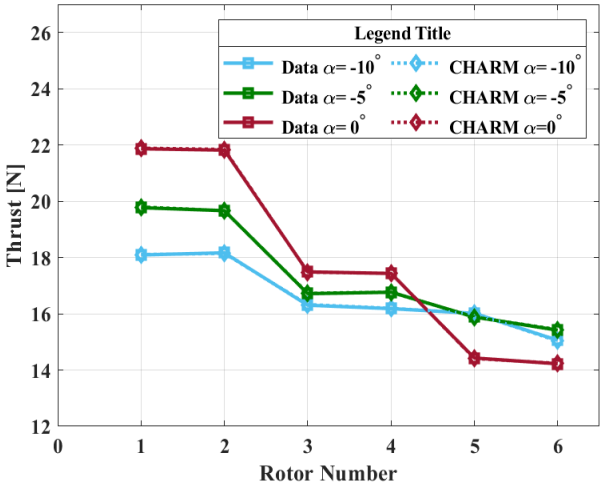

Figure 32. Measured and computed thrust values for individual rotors at c and pitch angle of -10, -5, and 0 deg for six-rotors, Short configuration.

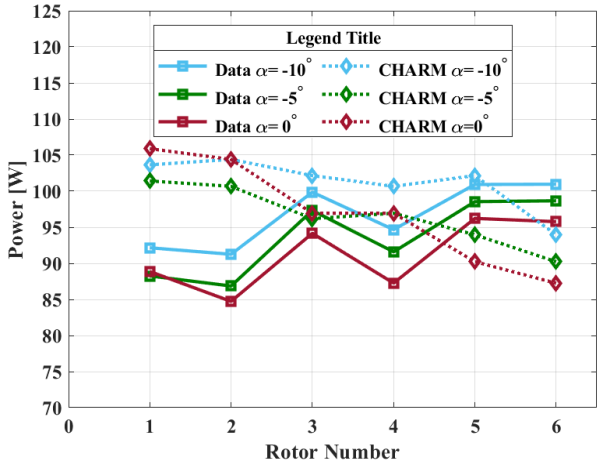

Figure 33. Measured and computed power values for individual rotors at 40 ft/s and pitch angle of -10, -5, and 0 deg for six-rotors, Short configuration.

Table 11. The summation of power for CHARM prediction and experimental data for six MTB rotors at the Short configuration at the wind tunnel in forward flight testing at speed of 20 ft/s and 40 ft/s.

V [ft/s]	Pitch [Deg]	Data, ∑ P[W]	CHARM, ∑ P[W]
19.89	-10	561.59	544.36
20.20	-5	555.02	539.89
19.76	0	543.18	510.80
40.07	-10	579.83	607.00
39.44	-5	561.25	579.41
40.28	0	547.02	581.65

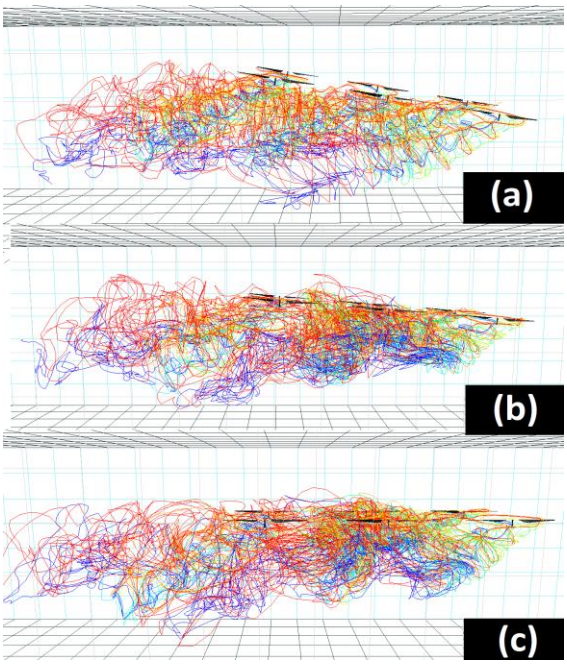

Figure 34. Simulated wake interactions for the six-rotor - Short configuration: (a) -10 deg (b) -5 deg, and (c) 0 deg pitch angle at forward flight of 20 ft/s.

Table 12. The discrepancy of power between the CHARM prediction and data for six MTB rotors at the Short configuration in the wind tunnel at 20ft/s.

V [ft/s]	α [°]	Power Discrepancy% R #1	R #2	R #3	R #4	R #5	R #6
19.9	-10	12.31	-5.71	2.05	-3.96	-3.29	15.86
20.2	-5	12.87	-0.38	-1.22	-6.75	-9.11	21.01
19.8	0	4.65	-0.15	-0.38	4.01	4.08	22.51
40.1	-10	-12.47	-14.41	-2.30	-6.33	-1.22	6.94
39.4	-5	-14.91	-15.90	1.16	-5.84	4.66	8.55
40.3	0	-19.15	-23.22	-2.96	-11.10	6.23	8.91

Results for the Six-Rotor, Tall Configuration

The measured thrust and power along with the CHARM prediction values for six-rotors in the Tall configuration at the pitch angles of 0, -5, -10 deg are shown in Figures 36-39 for speeds of 20 and 40 ft/s, respectively.

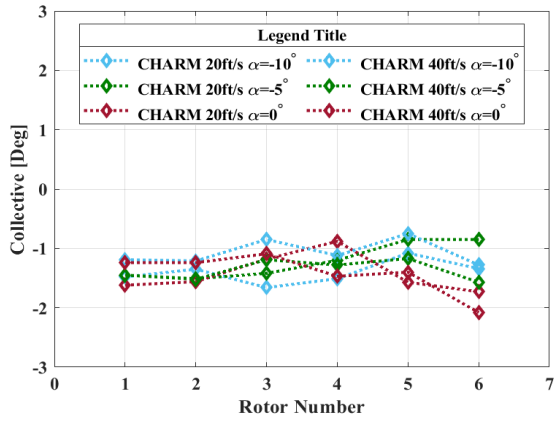

Figure 35. The collective values for individual rotors at pitch angle of -10, -5, and 0 deg, for six-rotors, Tall configuration in forward flight of 20 ft/s and 40 ft/s.

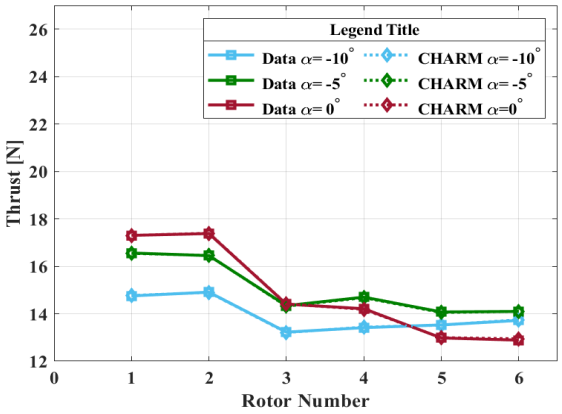

Figure 36. Measured and computed thrust values for individual rotors at 20 ft/s and pitch angle of -10, -5, and 0 deg for six-rotors, Tall configuration.

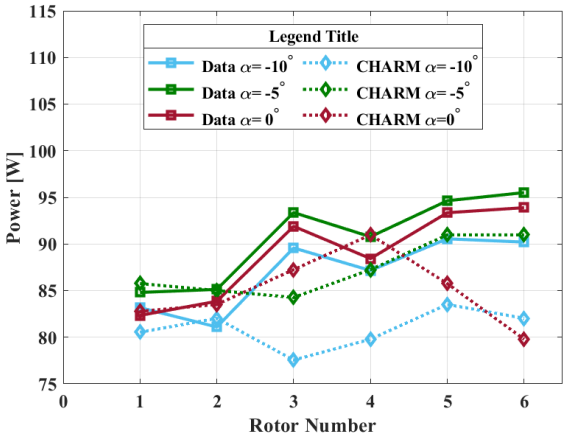

Figure 37. Measured and computed power values for individual rotors at 20 ft/s and pitch angle of -10, -5, and 0 deg for six-rotors, Tall configuration.

Also, the corresponding collective values in forward flight speed of 20 and 40 ft/s were shown in Figure 35. At the forward flight of 20 ft/s, experimental data shows that the highest power was achieved at a pitch angle of -5 degrees. This behavior was accurately predicted in CHARM. It is reasonable to expect the highest power value at a pitch angle

of -10 degrees due to decreasing the chance of the rotor's wake interactions as shown by the results in Table 13.

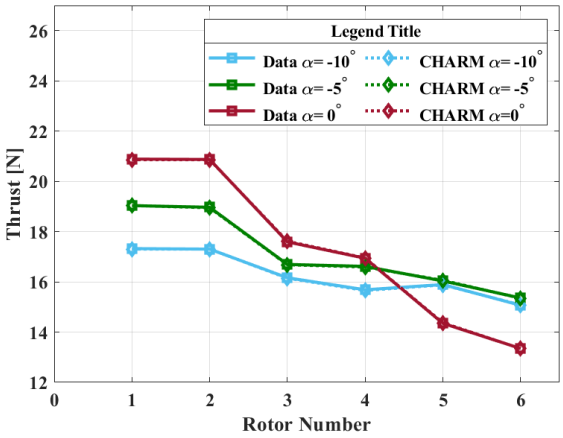

Figure 38. Measured and computed thrust values for individual rotors at 40 ft/s and pitch angle of -10, -5, and 0 deg for six-rotors, Tall configuration.

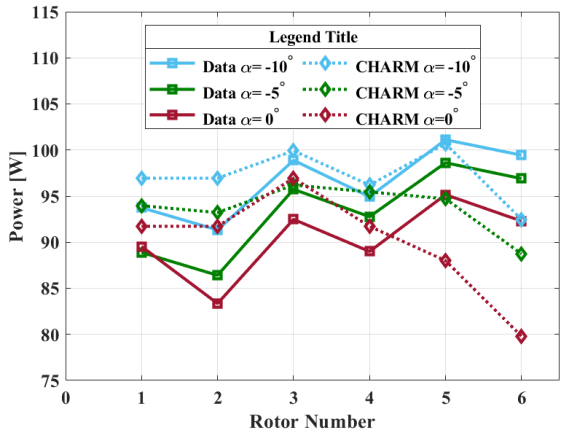

Figure 39. Measured and computed power values for individual rotors at 40 ft/s and pitch angle of -10, -5, and 0 deg for six-rotors, Tall configuration.

Table 13. The summation of power for CHARM prediction and experimental data for six MTB rotors at the Tall configuration at the wind tunnel in forward flight testing at speed of 20 ft/s and 40 ft/s.

V [ft/s]	Pitch [Deg]	Data, ∑ P[W]	CHARM, ∑ P[W]
20.73	-10	521.76	485.45
20.31	-5	544.23	524.23
20.11	0	533.77	510.06
40.01	-10	579.43	583.14
39.97	-5	559.31	562.26
39.94	0	541.80	539.89

However, at the Tall configurations, the back rotors (i.e., rotors 5 and 6) were much closer to the ceiling; therefore, these results might indicate the wall effect in the measurements and the simulations. The discrepancy between the experimental data and CHARM for the individual rotors was determined for this configuration at each pitch angle. The results are presented in Table 14. The average discrepancy at each pitch angle for the experimental and CHARM predictions at different pitch angles has been presented in Appendix C.

Table 14. The discrepancy of power between the CHARM prediction and experimental data for six MTB rotors at the Tall configuration at the wind tunnel in forward.

		Power Discrepancy%					
V [ft/s]	α [°]	R #1	R #2	R #3	R #4	R #5	R #6
20.7	-10	3.18	-1.14	13.42	8.45	7.77	9.06
20.3	-5	-1.12	0.14	9.75	3.89	3.87	4.75
20.1	0	-0.52	0.40	5.06	-2.87	8.14	15.02
40.0	-10	-3.42	-6.15	-1.05	-1.33	0.44	7.01
39.9	-5	-5.71	-7.88	-0.48	-2.89	3.97	8.42
39.9	0	-2.44	-10.05	-4.83	-3.07	7.53	13.54

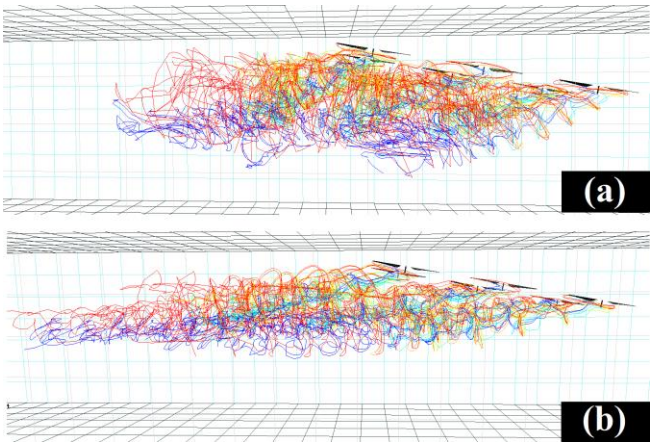

Figure 40. Six-rotor, Tall configuration: wake interactions at -10 deg pitch angle (a) 20 ft/s, (b) 40 ft/s.

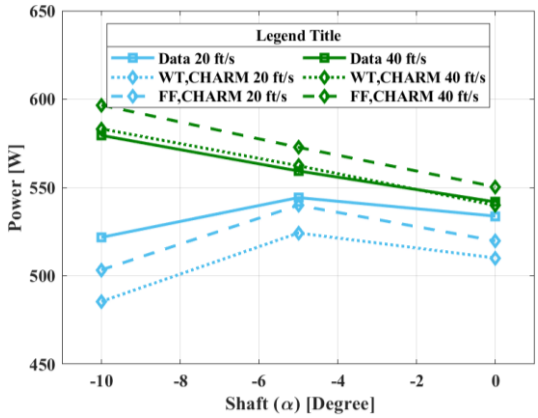

Figure 41. Power comparison between the data, wind tunnel (WT) prediction and the free field (FF) prediction for six-rotor cases in the Tall configuration.

Regardless of the results at 20 ft/s, the 40 ft/s in the Tall configuration produced the highest power at the -10 degrees pitch angle. The wake interactions were visualized at -10 deg for both 20 and 40 ft/s. This visualization showed that at a forward flight speed of 40 ft/s, rotors wakes convected downstream faster than at 20 ft/s which decreased rotors wake interactions – see Figure 40. The prediction results showed a

difference that could indicate wall effect. Comparing CHARM simulation results with and without wind tunnel walls can help understand this behavior. Figure 41 shows the experimental data, CHARM wind tunnel (WT), and CHARM free-field (FF) predictions for six-rotors in forward flight. The free-field predictions show better agreement with experimental data at the lower tunnel speed. This result indicates that the wind tunnel presence has a smaller effect on the experimental results at the lower speed. However, these results show a neglectable wall effect at the higher tunnel speed across the pitch angles, which complies with the observation of the rotor's wake in Figure 40.

DISCUSSION

Table 15 presents the power discrepancy between the experimental data and CHARM predictions at different pitch angles and forward flight speeds for both trimmed cases and fixed collective results. Even though CHARM simulations did not consider the test stand effect and needed further changes on the simulation setting, the power discrepancy was less than 10%, and the outcomes were still very promising.

Table 15. Absolute average discrepancy of Power between experimental data and CHARM with trimmed rotor and fixed collective.

Cases	Ave. Discrepancy% Trimmed Rotor	Ave. Discrepancy% Fixed Collective
Single Rotor	6.84	11.74
Two Rotors	6.57	11.84
Four Rotors	9.42	7.74
Six Rotors (Short)	8.24	8.69
Six Rotors (Tall)	5.24	6.60

The two-rotor and four-rotor case results show similar but unexpected trends. The left and right rotors are expected to experience similar thrust and power values. While the collective and thrust values for the left and right rotor were similar for CHARM and measured data, the power value was different, which indicated asymmetry in the aerodynamics. Also, the measured and predicted power showed a negative correlation between the left and right rotors in two-rotor and four-rotor cases which need more exploration (perhaps reflecting randomness in the source of the left-right asymmetry). In the result of the six-rotor case, the predicted collective is varying more in the Short configuration. For Tall and Short configurations at -10-deg pitch angle, the collective prediction remains at -1 degree, and variation near -1 deg was observed for the -5 and 0-deg pitch angle, indicating interference in the measurements. The measurements showed that the rear rotors generate less thrust while the power increases due to interference, but CHARM power predictions are more complex, see Figure 42 and Figure 43. Rear rotors experienced lower thrust due to inflow from front rotors, and power change due to the change of induced velocity from the front rotors and the change in thrust value. For this study, each rotor case was run at 50 revolutions, and the power and thrust values presented in this paper was the result of the last revolution.

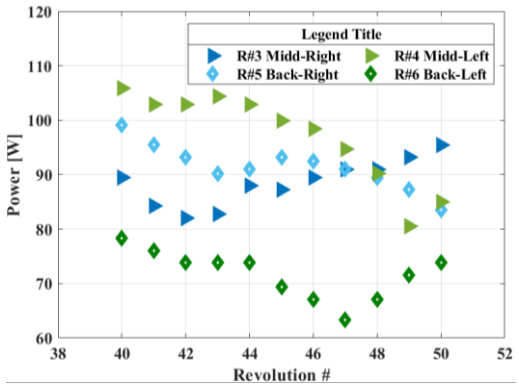

Figure 42. The power values for the last 10 revolution of the six-rotor case at Short configuration and 0 deg pitch angle at the wind tunnel speed of 20 ft/s.

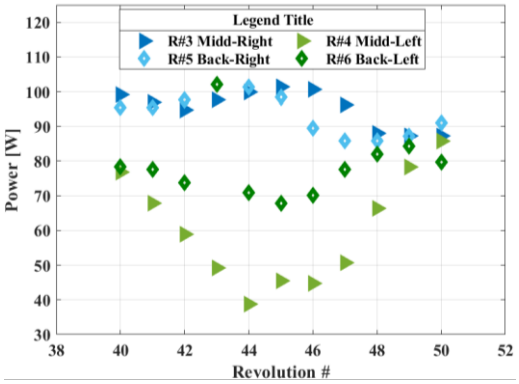

Figure 43. The power values for the last 10 revolution of the six-rotor case at Tall configuration and 0 deg pitch angle at the wind tunnel speed of 20 ft/s.

The CHARM simulation shows evidence of the unsteady wake, which suggests that the number of revolutions for each simulation run should be increased to mitigate this behavior. As such, using the average value over the last 5 to 10 revolutions could improve the results. These results indicate that further study is required to examine the data and explore the options in CHARM predictions in more detail to improve understanding of the rotor wake interference. Figures 44-49 show the average power between the front rotors (Rotor #1 and Rotor #2), middle rotors (Rotor #3 and Rotor #4), and back rotors (Rotor #5 and Rotor #6). Averaging the power values for the front, middle, and back rotors highlights the rotor wake interference between the front, middle, and rear rotors by minimizing the left/right asymmetry effect presented on measured and predicted results. The experimental data show a very similar trend regardless of the wind tunnel speed or the configuration's pitch angle. The experimental data shows that power values increase from the front rotor to the back rotors due to the rotor wake interaction. Also, data show that at forward flight of 40 ft/s, the Tall configuration and Short configuration have similar power values; however, CHARM predicted higher power values for the Short configuration, which could be due to the presence of the wall in the analysis. For forward flight of 20 ft/s, the measured data still follow similar trends as the 40ft/s, but CHARM prediction show more variation in the result.

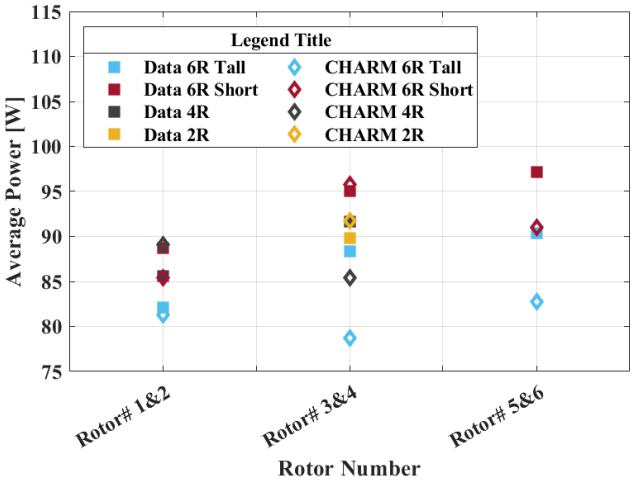

Figure 44. The average power of front, middle and back rotors at different MTB configuration at tunnel speed of 20 ft/s and -10 deg pitch angle.

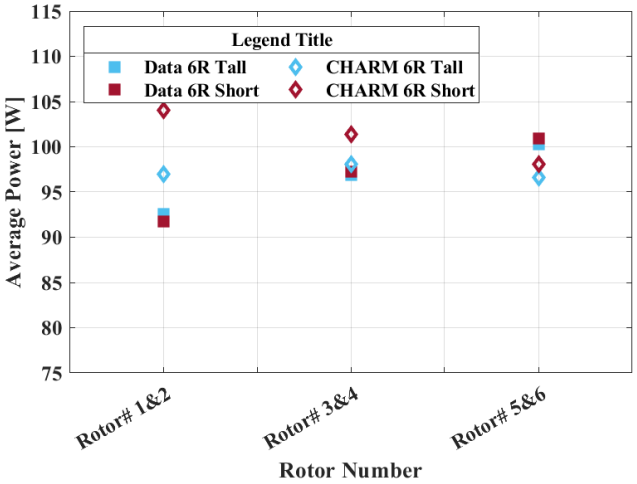

Figure 47. The average power of front, middle and back rotors at different MTB configuration at tunnel speed of 40 ft/s and -10 deg pitch angle.

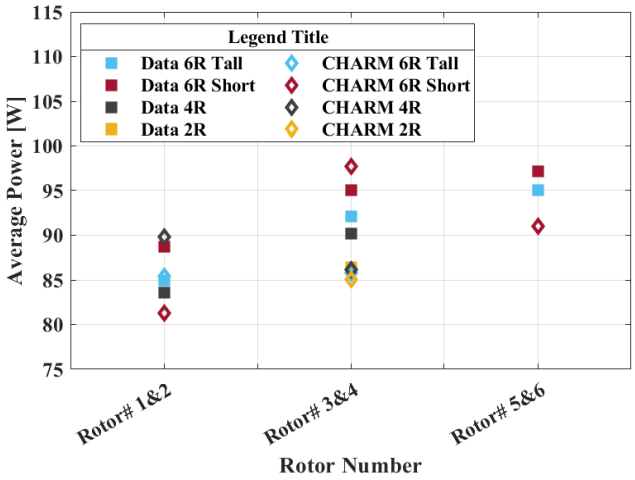

Figure 45. The average power of front, middle and back rotors at different MTB configuration at tunnel speed of 20 ft/s and -5 deg pitch angle.

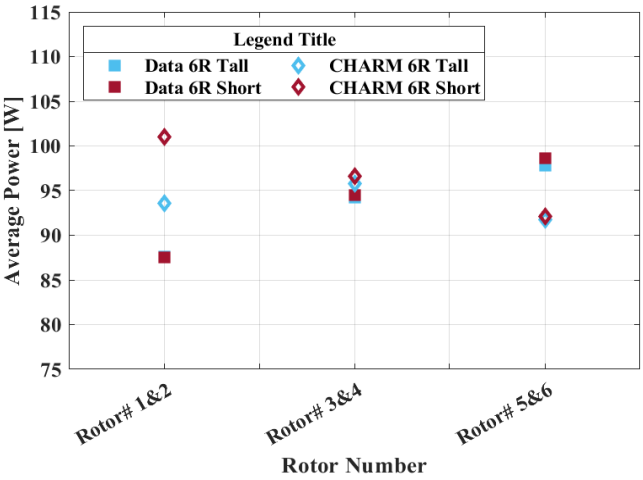

Figure 48. The average power of front, middle and back rotors at different MTB configuration at tunnel speed of 40 ft/s and -5 deg pitch angle.

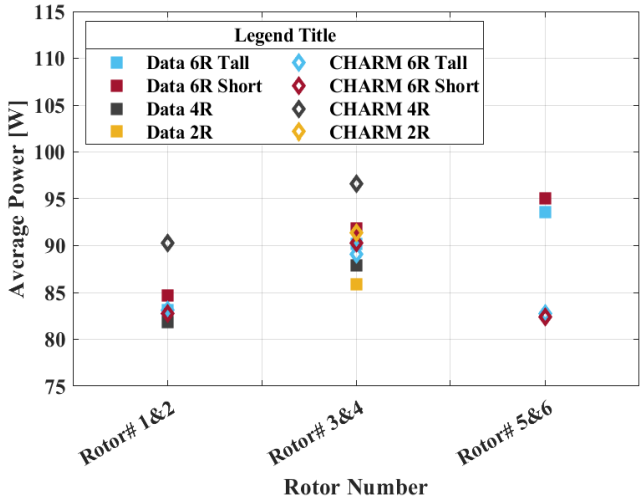

Figure 46. The average power of front, middle and back rotors at different MTB configuration at tunnel speed of 20 ft/s and 0 deg pitch angle.

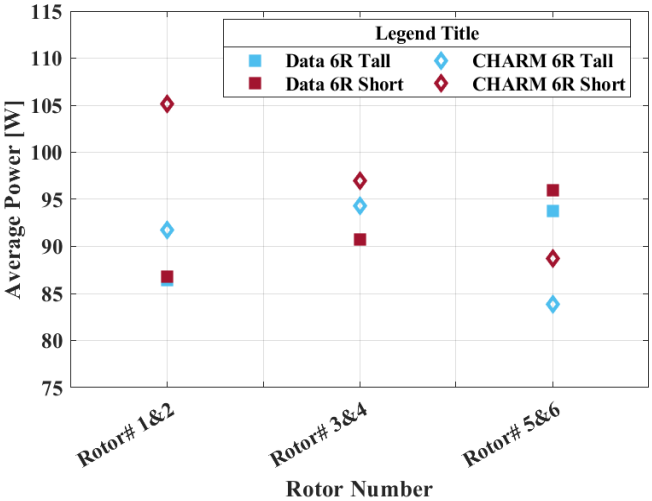

Figure 49. The average power of front, middle and back rotors at different MTB configuration at tunnel speed of 40 ft/s and 0 deg pitch angle.

CONCLUSIONS

The purpose of the research was to develop predictions of the 2019 MTB wind tunnel test data using CHARM. In the CHARM software, the vortex panel method was used to calculate wind tunnel effects. In addition, the Hierarchical Fast Vortex approach was used to model wakes and determine aerodynamic interactions between the rotors and the wind tunnel walls. CHARM was advantageous for this research study due to its limited usage of CPU and memory compared to other fully resolved CFD tools. In this study, individual rotors were trimmed to the measured thrust values and an increment of -0.003 was applied to c_d values in the airfoil tables. The CHARM simulations included the 7- by 10-Foot Wind Tunnel test section walls and also simulated the MTB rotors in the free field. The simulations did not include the test stand, and still, the outcomes were very promising. Based on the results obtained from this study, the key findings can be summarized as follows:

1) Simulations of trimmed rotors provided better predictions of the power values compared to simulation of rotors with fixed collective except for the four-rotor cases, Table 15. This outcome requires further study to explain this phenomenon.

2) The number of rotors is not an indicator of a higher discrepancy between the experimental data and CHARM. For example, the six-rotor case at the Tall configuration had the lowest discrepancy.

3) The complexity of determining the minimum drag depends on various factors including Reynolds number, surface roughness, and flow conditions, among others. This warrants further study of the drag values to determine how to improve power predictions based on the coefficient of drag in the airfoil tables.

4) There is a possibility that CHARM overpredicted the induced power. Due to insufficient information, pinpointing the cause of this overall behavior requires further investigation.

5) Taking the average over multiple revolutions of the simulation results could improve the prediction comparison with measurements by mitigating the effects of the unsteady solution.

6) The airfoil tables were a potential source of error because the geometry of one rotor blade was used to generate the airfoil tables for all six-rotors. For future studies, the blades of all six rotors should be laser scanned to determine the geometrical differences between the rotors.

7) Other potential sources of error were the load cells, which need to be re-calibrated to minimize possible errors in experimental data measurement.

8) Having each of the six MTB rotors tested one at a time as a single rotor in future wind tunnel testing will improve understanding of rotor behavior and help identify rotor-to-rotor differences.

Overall, this research study has demonstrated that trimming the rotor and adjusting the drag coefficient values on the airfoil tables improve the CHARM prediction, and this process can be used to simulate other multirotor configurations.

FUTURE WORK

After calibrating the load cell and validating the CHARM settings, the measured data need to be re-examined to eliminate any possible discrepancies and improve the correlation. In addition, examining the airfoil table can benefit from the result of this research. Overall, more work needs to be done to examine the data, run CHARM, and understand the full capabilities of using CHARM for multirotor simulations to predict such complex rotor interactions.

Author contact: Dorsa Shirazi dorsa.shirazi@nasa.gov

APPENDIX A

The measured parameters used in the CHARM simulation are presented in Appendix A.

Table A1. The measured parameters used in the CHARM simulation.

MTB Config	Alpha [deg]	Rotor#	CT	Ω [rad /s]	Speed of Sound [ft/s]	ρ [slug/ft3]	WT Speed [ft/sec]
1 Rotor, Short	-10	2	0.01008	209.45941	1135.97341	0.00231	20.29998
1 Rotor, Short	-5	2	0.01044	209.56298	1135.92374	0.00231	20.39706
1 Rotor, Short	0	2	0.01090	209.39336	1135.94754	0.00231	20.36606
1 Rotor, Short	-10	2	0.01129	209.42125	1137.82614	0.00244	39.83185
1 Rotor, Short	-5	2	0.01223	209.55991	1137.82614	0.00244	39.33382
1 Rotor, Short	0	2	0.01324	209.30812	1137.82614	0.00244	39.34242
MTB Config	Alpha [deg]	Rotor#	CT	Ω [rad /s]	Speed of Sound [ft/s]	ρ [slug/ft3]	WT Speed [ft/sec]
6 Rotor, Short	-10	1	0.00964	209.40124	1133.63664	0.00242	19.88723
6 Rotor, Short	-10	2	0.01021	209.49710	1133.63664	0.00242	19.88723
6 Rotor, Short	-10	3	0.00982	209.40625	1133.63664	0.00242	19.88723
6 Rotor, Short	-10	4	0.00967	209.41399	1133.63664	0.00242	19.88723
6 Rotor, Short	-10	5	0.00975	209.44802	1133.63664	0.00242	19.88723
6 Rotor, Short	-10	6	0.00872	209.33008	1133.63664	0.00242	19.88723
6 Rotor, Short	-5	1	0.01010	209.49756	1134.39952	0.00241	20.19742
6 Rotor, Short	-5	2	0.01069	209.40396	1134.39952	0.00241	20.19742
6 Rotor, Short	-5	3	0.00932	209.58578	1134.39952	0.00241	20.19742
6 Rotor, Short	-5	4	0.00968	209.49878	1134.39952	0.00241	20.19742
6 Rotor, Short	-5	5	0.00932	209.45379	1134.39952	0.00241	20.19742
6 Rotor, Short	-5	6	0.00856	209.41656	1134.39952	0.00241	20.19742
6 Rotor, Short	0	1	0.01088	209.55161	1135.35240	0.00241	19.75716
6 Rotor, Short	0	2	0.01111	209.35508	1135.35240	0.00241	19.75716
6 Rotor, Short	0	3	0.00910	209.19001	1135.35240	0.00241	19.75716
6 Rotor, Short	0	4	0.00946	209.40132	1135.35240	0.00241	19.75716
6 Rotor, Short	0	5	0.00909	209.40745	1135.35240	0.00241	19.75716
6 Rotor, Short	0	6	0.00822	209.47872	1135.35240	0.00241	19.75716
6 Rotor, Short	-10	1	0.01157	209.51347	1141.25896	0.00239	40.07122
6 Rotor, Short	-10	2	0.01162	209.51394	1141.25896	0.00239	40.07122
6 Rotor, Short	-10	3	0.01044	209.42952	1141.25896	0.00239	40.07122
6 Rotor, Short	-10	4	0.01035	209.49830	1141.25896	0.00239	40.07122
6 Rotor, Short	-10	5	0.01024	209.51435	1141.25896	0.00239	40.07122
6 Rotor, Short	-10	6	0.00964	209.42239	1141.25896	0.00239	40.07122
6 Rotor, Short	-5	1	0.01268	209.47323	1142.60121	0.00238	39.43707
6 Rotor, Short	-5	2	0.01262	209.41047	1142.60121	0.00238	39.43707
6 Rotor, Short	-5	3	0.01071	209.49374	1142.60121	0.00238	39.43707
6 Rotor, Short	-5	4	0.01075	209.42613	1142.60121	0.00238	39.43707
6 Rotor, Short	-5	5	0.01018	209.50840	1142.60121	0.00238	39.43707
6 Rotor, Short	-5	6	0.00987	209.56779	1142.60121	0.00238	39.43707
6 Rotor, Short	0	1	0.01405	209.49347	1144.32818	0.00238	40.27893
6 Rotor, Short	0	2	0.01401	209.49996	1144.32818	0.00238	40.27893
6 Rotor, Short	0	3	0.01122	209.59381	1144.32818	0.00238	40.27893
6 Rotor, Short	0	4	0.01121	209.40960	1144.32818	0.00238	40.27893
6 Rotor, Short	0	5	0.00926	209.52841	1144.32818	0.00238	40.27893
6 Rotor, Short	0	6	0.00914	209.41998	1144.32818	0.00238	40.27893
MTB Config	Alpha [deg]	Rotor#	CT	Ω [rad /s]	Speed of Sound [ft/s]	ρ [slug/ft3]	WT Speed [ft/sec]
4 Rotor, Short	-10	1	0.01059	209.36381	1154.24475	0.00232	20.29636
4 Rotor, Short	-10	2	0.01027	210.01670	1154.24475	0.00232	20.29636
4 Rotor, Short	-10	3	0.00892	209.49364	1154.24475	0.00232	20.29636
4 Rotor, Short	-10	4	0.00952	209.52137	1154.24475	0.00232	20.29636
4 Rotor, Short	-5	1	0.01126	209.33545	1154.05736	0.00231	20.42222
4 Rotor, Short	-5	2	0.01094	209.43799	1154.05736	0.00231	20.42222
4 Rotor, Short	-5	3	0.00884	209.37412	1154.05736	0.00231	20.42222
4 Rotor, Short	-5	4	0.01003	209.48605	1154.05736	0.00231	20.42222
4 Rotor, Short	0	1	0.01170	209.41445	1153.68248	0.00230	20.43753
4 Rotor, Short	0	2	0.01152	209.42100	1153.68248	0.00230	20.43753
4 Rotor, Short	0	3	0.00889	209.38309	1153.68248	0.00230	20.43753
4 Rotor, Short	0	4	0.00965	209.41622	1153.68248	0.00230	20.43753
MTB Config	Alpha [deg]	Rotor#	CT	Ω [rad /s]	Speed of Sound [ft/s]	ρ [slug/ft3]	WT Speed [ft/sec]
2 Rotor, Short	-10	3	0.01021	208.86895	1129.89284	0.00241	20.10200
2 Rotor, Short	-10	4	0.01027	209.42286	1129.89284	0.00241	20.10200
2 Rotor, Short	-5	3	0.01024	209.39867	1130.08915	0.00241	19.95945
2 Rotor, Short	-5	4	0.01063	209.55606	1130.08915	0.00241	19.95945
2 Rotor, Short	0	3	0.01082	209.34484	1130.79517	0.00241	19.62403
2 Rotor, Short	0	4	0.01100	209.51405	1130.79517	0.00241	19.62403

MTB Config	Alpha [deg]	Rotor#	CT	Ω [rad /s]	Speed of Sound [ft/s]	ρ [slug/ft3]	WT Speed [ft/sec]
4 Rotor, Short	-10	1	0.01059	209.36381	1154.24475	0.00232	20.29636
4 Rotor, Short	-10	2	0.01027	210.01670	1154.24475	0.00232	20.29636
4 Rotor, Short	-10	3	0.00892	209.49364	1154.24475	0.00232	20.29636
4 Rotor, Short	-10	4	0.00952	209.52137	1154.24475	0.00232	20.29636
4 Rotor, Short	-5	1	0.01126	209.33545	1154.05736	0.00231	20.42222
4 Rotor, Short	-5	2	0.01094	209.43799	1154.05736	0.00231	20.42222
4 Rotor, Short	-5	3	0.00884	209.37412	1154.05736	0.00231	20.42222
4 Rotor, Short	-5	4	0.01003	209.48605	1154.05736	0.00231	20.42222
4 Rotor, Short	0	1	0.01170	209.41445	1153.68248	0.00230	20.43753
4 Rotor, Short	0	2	0.01152	209.42100	1153.68248	0.00230	20.43753
4 Rotor, Short	0	3	0.00889	209.38309	1153.68248	0.00230	20.43753
4 Rotor, Short	0	4	0.00965	209.41622	1153.68248	0.00230	20.43753
MTB Config	Alpha [deg]	Rotor#	CT	Ω [rad /s]	Speed of Sound [ft/s]	ρ [slug/ft3]	WT Speed [ft/sec]
2 Rotor, Short	-10	3	0.01021	208.86895	1129.89284	0.00241	20.10200
2 Rotor, Short	-10	4	0.01027	209.42286	1129.89284	0.00241	20.10200
2 Rotor, Short	-5	3	0.01024	209.39867	1130.08915	0.00241	19.95945
2 Rotor, Short	-5	4	0.01063	209.55606	1130.08915	0.00241	19.95945
2 Rotor, Short	0	3	0.01082	209.34484	1130.79517	0.00241	19.62403
2 Rotor, Short	0	4	0.01100	209.51405	1130.79517	0.00241	19.62403

APPENDIX B

The additional Vortex-X flow visualizations can be found in Appendix B.

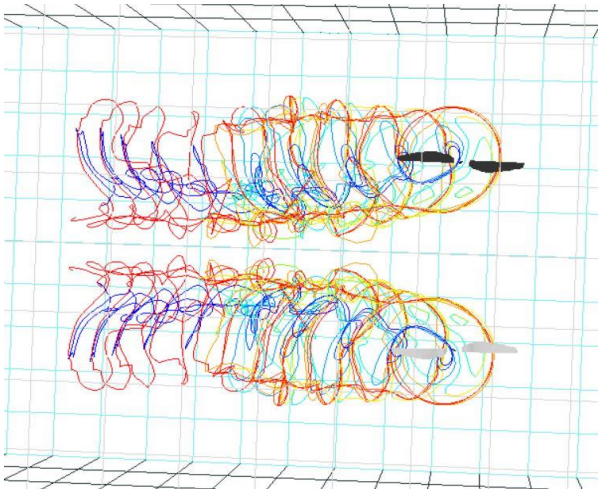

Figure B1. Two-rotor cases at forward flight 20 ft/s in wind tunnel with pitch-10 degrees.

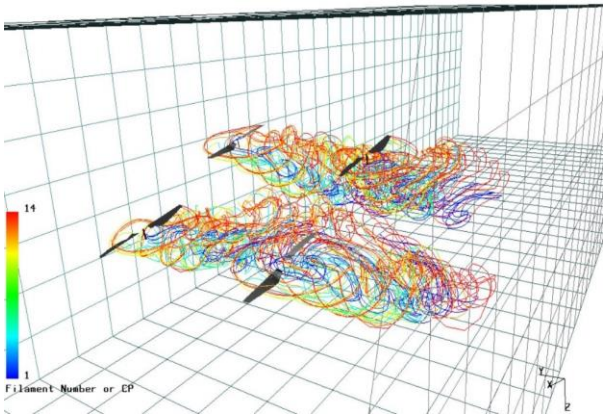

Figure B2. Flow visualization of rotors numbers 1-4 in the short rotor configuration, at the -10 degrees pitch angle, and with a wind tunnel speed of 20 ft/s.

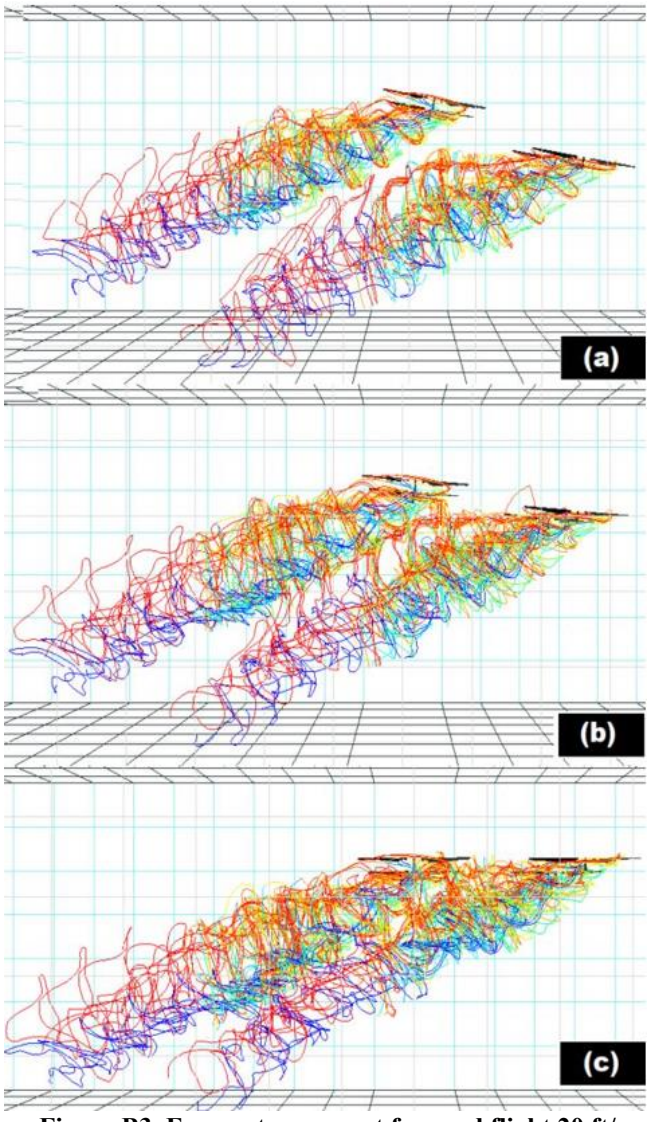

Figure B3. Four-rotor cases at forward flight 20 ft/s in wind tunnel - side view - pitch angle (a) -10 degrees (b) -5 degrees (c) 0 degrees.

APPENDIX C

The summation of the experimental and CHARM predictions power at the pitch angle of -10, -5, and 0 degrees are presented in Appendix C.

Table C1. The summation of power CHARM prediction and experimental data for two MTB rotors at the wind tunnel in forward flight testing at speed of 20ft/s.

V [ft/s]	Pitch [Deg]	Data, ∑ P[W]	CHARM, ∑ P[W]
20.10	-10	179.62	183.44
19.96	-5	172.86	170.02
19.82	0	171.67	182.70

Table C2. The summation of power for CHARM prediction and experimental data for four MTB rotors at the wind tunnel in forward flight speed of 20ft/s.

V [ft/s]	Pitch [Deg]	Data, ∑ P[W]	CHARM, ∑ P[W]
20.30	-10	354.42	348.99
20.42	-5	347.54	351.97
20.44	0	339.54	373.60

Table C3. The average discrepancy of power between the CHARM prediction and experimental data for four MTB rotors at the wind tunnel in forward flight testing at speed of 20ft/s.

V [ft/s]	Pitch [Deg]	Power Ave. Discrepancy%
20.30	-10	6.30
20.42	-5	9.62
20.44	0	12.33

Table C4. The average discrepancy of power between the CHARM prediction and experimental data for six MTB rotors at the Tall configuration at the wind tunnel in forward flight testing at speed of 20ft/s and 40 ft/s.

V [ft/s]	Pitch [Deg]	Power Ave. Discrepancy%
20.73	-10	7.17
20.31	-5	3.92
20.11	0	5.34
40.01	-10	3.23
39.97	-5	4.89
39.94	0	6.91

APPENDIX D

The additional figures for power versus revolution numbers are presented in Appendix D. The figure shows the power values for the last ten revolutions.

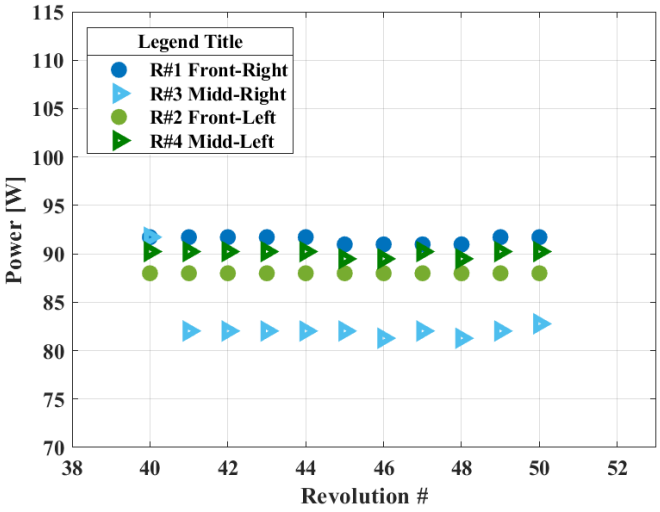

Figure D1. CHARM power variation over last 10 rotor revolutions (total 50 revolutions) with wind tunnel walls: pitch angle of -10 deg; 20 ft/s; four-rotor case.

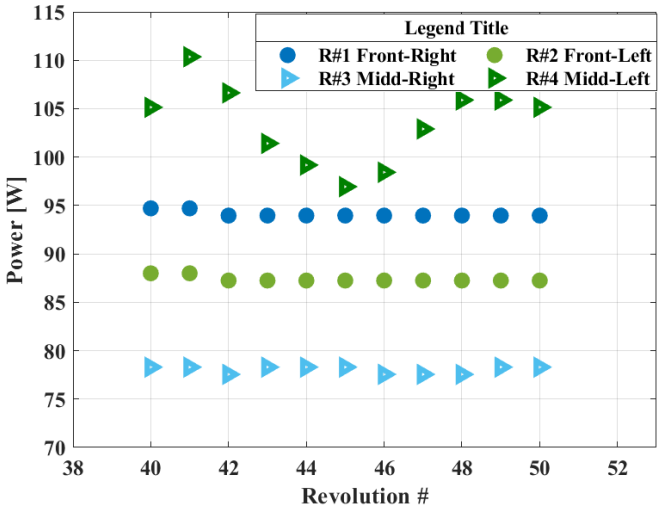

Figure D2. CHARM power variation over last 10 rotor revolutions (total 50 revolutions) with wind tunnel walls: pitch angle of -5 deg; 20 ft/s; four-rotor case.

ACKNOWLEDGMENTS

The author would like to express profound gratitude to Gloria Yamauchi, who guided her in all steps of this project, and Wayne Johnson, who gave so very generously of his knowledge and time. The author would like to thank Carl Russell, Christopher Silva, Sarah Conley, Ethan Romander, Dan Wachspress, Thomas Norman, and Dorcas Kaweesa. The author would like to acknowledge William Warmbrodt for his continued support and Kristen Kallstrom, who developed the airfoil tables for the MTB rotors.

REFERENCES

1. Russell, C.; Willink, G.; Theodore, C.; Jung, J.; and Glasner, B. "Wind Tunnel and Hover Performance Test Results for Multicopter UAS Vehicles." NASA TM 2018-219758, February 2018.
2. Russell, C., and Conley, S. “The Multirotor Test Bed – A New NASA Test Capability for Advanced VTOL Rotorcraft Configurations,” Vertical Flight Society 76th Annual Forum and Technology Display, October 2020.
3. Conley, S, and Shirazi, D. “Comparing Simulation Results from CHARM and RotCFD to the Multirotor Test Bed Experimental Data”, AIAA Aviation Forum 2021- AIAA-2021-2540, August 2021.
4. Conley, S., Russell, C., Kallstrom, K., Koning, W., and Romander, E., “Comparing CFD Predictions of the Multirotor Test Bed with Experimental Results,” presented at the VFS 76th Annual Forum and Technology Display, Virginia Beach, VA, October 2020.
5. Wachspress, D.A.; Quackenbush, T.R.; and Boschitsch, A.H. "Rotorcraft Interactional Aerodynamics with Fast Vortex/Fast Panel Methods," Journal of the American Helicopter Society, Volume 48, Number 4, 1 October 2003, pp. 223-235(13).
6. Quackenbush, T., Boschitsch, A., Wachspress, D., McKillip Jr, R. and MacNichol, A. “Fast analysis methods for surface-bounded flows with applications to rotor wake modeling”, American Helicopter Society 52nd Annual Forum, Washington DC, June 1996.
7. Wachspress, D. A., Quackenbush, T. R., and Boschitsch, A. H., “First-Principles Free-Vortex Wake Analysis for Helicopters and Tiltrotors,” American Helicopter Society 59th Annual Forum, Phoenix, AZ, May 2003.
8. Shirazi, D., “Wake Simulation of the Multirotor Test Bed and Validation of CHARM Software,” NASA TM, 2022 (to be published).